An $\mathcal{H}_\infty$ Power Flow Approach to Control of Uncertain Structures

by

Douglas G. MacMartin

B.A.Sc. University of Toronto (1987)

SUBMITTED IN PARTIAL FULFILLMENT OF THE
REQUIREMENTS FOR THE DEGREE OF

Master of Science
in
Aeronautics and Astronautics
at the
Massachusetts Institute of Technology
February 1990

Signature of Author _____
Department of Aeronautics and Astronautics
October 27, 1989

Certified by _____
Professor Steven R. Hall
Thesis Supervisor, Department of Aeronautics and Astronautics

Accepted by _____
Professor Harold Y. Wachman
Chairman, Department Graduate Comittee

An $\mathcal{H}_\infty$ Power Flow Approach to Control of Uncertain Structures

by

Douglas G. MacMartin

Submitted to the Department of Aeronautics and Astronautics
on October 27, 1989 in partial fulfillment of the
requirements for the Degree of Master of Science in
Aeronautics and Astronautics

Abstract

A technique is described for generating guaranteed stable control laws for uncertain, modally dense structures with collocated sensors and actuators. By ignoring the reverberant response created by reflections from other parts of the structure, a dereverberated mobility model can be developed which accurately models the local dynamics of the structure. This is similar in many respects to a wave based model, but can treat more general structures, not only those that can be represented as a collection of waveguides. This model can be determined directly from transfer function data using an analysis technique based on the complex cepstrum. In order to minimize the effect of disturbances propagating through the structure, the power dissipated by the controller is maximized in an $\mathcal{H}_\infty$ sense. This guarantees that the controller is positive real, and thus that the system will remain stable for any structural uncertainty. The approach is demonstrated for several examples. Experimental results on a beam in bending are presented. The controller based on this approach is much more effective than simple collocated rate feedback. Significant damping was added to many modes of the structure, without requiring a detailed or high order model of the beam.

Thesis Supervisor: Dr. Steven R. Hall, Sc.D.,
Boeing Assistant Professor of
Aeronautics and Astronautics

Acknowledgements

There are many people who in some way contributed to this thesis. In particular, I would like to thank my advisor, Professor Steven R. Hall, without whom this certainly would not have been possible. The credit for many of the ideas presented here should go to Steve. I would also like to thank Dr. David Miller and Professor Andy von Flotow for many interesting and useful conversations, and for providing additional insight into the approach presented here, and the various solutions that I obtained. Dave's assistance with the experiment is also greatly appreciated. Experimental results could not have been obtained without both his previous work in setting up the equipment, and his assistance in the actual experimentation. Thanks also to Pablo Iglesias, who provided the $\mathcal{H}_\infty$ software used in this thesis. Finally, I would like to thank Jon and Vera and everyone else in the lab for their suggestions on this research, and for making this an enjoyable place to work.

This work was supported by the Air Force Office of Scientific Research under Grant no. AFOSR-88-0029 with Dr. Anthony K. Amos, and Dr. Haritos serving as technical monitors.

Contents

List of Figures

Chapter 1

Introduction

1.1 Motivation and Background

Broadband active control of flexible structures is difficult for several reasons. Structures tend to be very lightly damped, modally rich, and difficult to model in detail, due to their large sensitivity to parameter variations. It is well known [4] that for many applications, there are likely to be many flexible modes within the desired bandwidth of a structural control system. This is due in part to the light damping that would be anticipated, for example in large space structures, which implies that many modes can contribute to the performance. Also, performance requirements may push the bandwidth higher directly, for example in noise control of machinery, where the bandwidth must clearly include acoustic frequencies, and therefore many flexible modes.

One of the problems associated with broadband control of structures is the uncertainty in the plant model. A state space model of a structure must be at best an approximation, since the true structure is infinite-dimensional. Finite element methods are typically used to model a structure, and are sometimes capable of modelling the lowest modes quite accurately. However, in the region of high modal density, any model is likely to be highly inaccurate. Models of structures with

closely spaced modes in particular tend to be extremely sensitive to small parameter changes, in their prediction of natural frequencies, and especially in their prediction of mode shapes. As a result, the actual structure to which the control will eventually be applied may differ significantly from the model for which it was designed. Thus some knowledge about the uncertainty must be taken into account when designing the controllers.

A variety of approaches have been used to deal with uncertainty in the plant model. One typical approach is to treat the uncertainty as a multiplicative error which is totally unstructured. Bounds are specified on the magnitude of the perturbation, while the phase is assumed unknown. In this case, stability can be guaranteed by requiring that the closed loop complementary sensitivity be bounded above by the inverse of the maximum singular value of the uncertainty bound [11]. Thus for the nominal plant $G(s)$, if the true plant is given by

$$G_{\text{true}}(s) = (I + L(s))G(s) \tag{1.1}$$

then the system is stable with feedback matrix $K(s)$ if

$$\bar{\sigma}\left(G(j\omega)K(j\omega)(I + G(j\omega)K(j\omega))^{-1}\right) < \frac{1}{L_m(\omega)} \quad \forall\ \omega \tag{1.2}$$

where $\bar{\sigma}(\cdot)$ is the maximum singular value, and L_m is a function which satisfies

$$L_m(j\omega) \geq |\bar{\sigma}(L(j\omega))| \quad \forall\ \omega \tag{1.3}$$

This approach is reasonable for truly unstructured uncertainty such as unmodelled high frequency dynamics, and also may not be overly conservative for some parametric, or structured uncertainty. However, for lightly damped, modally dense systems, this approach will be extremely conservative. If the poles and zeroes are close together, a small parameter error may result in the true pole lying at the frequency of the modelled zero. The model error required in this case is significantly larger than the plant itself [7]. This would imply that almost no control can be

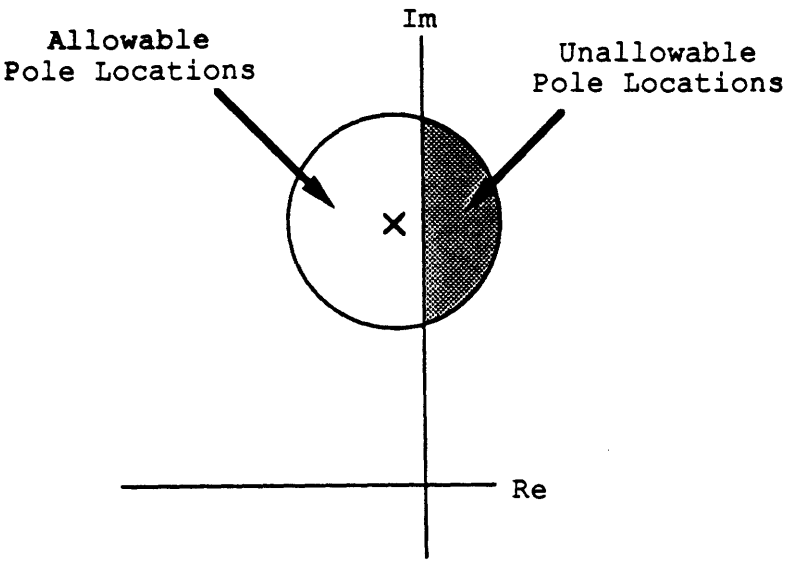

Figure 1.1: No knowledge of uncertainty direction may result in physically impossible pole locations

applied in this region, and thus that nothing can be done to damp this mode. The problem lies in the assumption of no knowledge about the direction of uncertainty. In fact, since the structure is known to be stable yet lightly damped, there can be far more uncertainty in the imaginary part of the pole location, or frequency, than in the real part [5], as shown in Figure 1.1. Though the relative error in the real part is large, the absolute error is small compared to the frequency, since right half plane poles are not possible.

This conservative stability robustness test can be relaxed by taking advantage of the positivity of structures. A transfer matrix G is positive real if

$$G(s) + G^T(-s) \geq 0 \quad \forall \ \mathrm{Re}(s) > 0 \tag{1.4}$$

and strictly positive real if the first inequality is strict [1]. Any strictly positive real compensator will be stabilizing for any positive real plant. If the perturbation matrix L is defined as just the deviation of the plant from the positive real condition, then stability can be guaranteed if the compensator is both strictly positive real and

satisfies the earlier singular value test (Equations (1.2) and (1.3)) for this smaller perturbation [37].

Another approach for dealing with uncertainty in some parameters is the Maximum Entropy/Optimal Projection (MEOP) approach by Bernstein and Hyland [5]. The goal of MEOP is to force the LQG algorithm to provide a more robust controller, by including information about parametric uncertainty into the plant model. This is done by using a stochastic model of the plant uncertainty. This approach yields compensators with good performance over the entire range of parameters, at the expense of a cumbersome numerical algorithm. However, there is no guarantee of stability using this method. The μ-synthesis approach by Doyle [12] also allows for some structure in the uncertainty, and allows the performance to be optimized not just for the nominal model, but for any model within the specified uncertainty bounds. Control architectures such as HAC/LAC (High-Authority Control/Low-Authority Control) [2], hierarchic control [18,20], and many others such as [3], have been designed to deal with the spillover problems associated with uncertainty in modelling structures. Other approaches have also been developed to deal with control design for uncertain structures; a good review of many of these can be found in [25].

Many of these approaches to control design for uncertain structures begin with a large order, detailed nominal model of the structure, and deal with uncertainty by attempting to model it, as well as the nominal plant, in some fashion. However, if the nominal model contains significant error, then the detailed information it contains is meaningless, and has no effect other than to increase the computational burden associated with the control design. Indeed, for broadband control of a modally rich structure, the dimension of the plant required to model each mode may be prohibitive for many control design techniques. Instead, only the information that can be accurately modelled should be included in the description of the plant [5].

With this philosophy, there has been much research on the use of wave based

models for use in structural control. Early work in this field includes that of Vaughan [39], who identified a matched termination as being an appropriate control law for a beam, and gave suitable approximations for the implementation of the irrational transfer functions required. More recently, a number of researchers have done both theoretical [17,23,28,35,41] and experimental [29,32,33,40] work in wave-based control for structures. The assumption in all of this research is that the local dynamics can be accurately modelled, and that an effective control system can be derived based only on this information. The control derivations either attempt to eliminate reflection or transmission by controlling elements of the scattering matrix, or are optimal approaches, based on maximizing some quantity such as the power dissipation.

Mace [23] derives the control necessary to cancel the incoming disturbances by creating waves of opposite sign. This methodology can only be effectively applied to one-dimensional waveguides. For a Timoshenko beam, Hagedorn and Schmidt [17] maximize the power flow out of the beam to obtain 'energy valves' that allow energy to travel in one direction, but not the other. The modelling formalism of Miller *et al.* [28], or that of von Flotow [41] allows the analysis of somewhat more general structures, including any arbitrary network of waveguides. In this framework, control laws can be developed to set certain elements of the scattering matrix to zero, or to maximize the power flow out of the structure. The experimental results cited earlier have all applied wave control to beams. Von Flotow and Shäfer [40] designed control laws to modify elements of the scattering matrix, and compared their results with those for modal control. Optimal control techniques were tested by Miller and Hall [29].

These wave control methods have demonstrated that good performance can be achieved on a structure without requiring knowledge of uncertain information such as the modal frequencies. One drawback to many of the wave-based approaches is that they cannot always be applied to a general structure, at best being able to

treat networks of waveguides.

Of particular relevance to this thesis is the optimal control approach of Miller *et al.* [28]. The structure is represented as being composed of one-dimensional waveguides which meet at junctions, and only the junction at which the control acts is modelled. Using Weiner-Hopf techniques to ensure causality, Miller *et al.* maximize the frequency weighted power dissipation associated with the control. The drawback to this approach is that it will allow power to be generated at some frequencies in order to achieve greater power dissipation at other frequencies. If there is a mode of the system at such a frequency, it may be destabilized by this compensator. This problem is corrected by approximating the optimal compensator with a positive real form, which is guaranteed to be stabilizing. The final result, then, is suboptimal, because the positive real constraint is applied in a somewhat *ad hoc* manner. Thus while this design procedure is attractive, an approach which treats more general structures and provides a guarantee of stability is desired.

1.2 Approach

This thesis describes a new approach to the modelling and control of uncertain structures that will guarantee both stability robustness and performance robustness. Much of the material presented here has been summarized in a previous paper [24].

The goal is to obtain a compensator that will provide broadband damping to the structure. This might be used in conjunction with a low order modal compensator which could provide good performance on those modes that could be well modelled. Thus this could be used as the low authority controller in a HAC/LAC architecture [2], rather than the rate feedback typically used. Rate feedback is guaranteed to be stable, but it is not necessarily optimal. In general it is possible to add more damping to a structure than can be obtained through rate feedback [29].

The model used in this thesis is the dereverberated mobility at a collocated and

dual actuator/sensor pair [22]. Only that part of the response which is due to the local dynamics is retained in the model. This can be shown to correspond in the frequency domain to an averaging, or smoothing, of the transfer function. This model bears some relationship to the wave approach of [28], but it is more general, as it allows structures which are not networks of waveguides to be treated.

Since the driving point mobility of a structure is positive real, stability can be guaranteed by requiring that the compensator be positive real. This is assured by minimizing the maximum value over frequency of the power flow into the structure. This minimax problem can be reformulated as an H_∞ optimization problem, and then solved using existing software. This results in a compensator which dissipates power at all frequencies. Taking energy as the Lyapunov function shows that the closed loop system must be stable for all plants, provided that the sensors and actuators are not mismodelled. Extensions based on the results of Slater [37] to allow for actuator and sensor dynamics, time delays, or actuators and sensors that are not collocated, are possible but are not treated here.

1.3 Overview

The remainder of this thesis is divided into six chapters. Chapter 2 presents some of the necessary mathematical background. This includes some theory on H_∞ control, and results on spectral factorization from [15] that will be needed in Chapter 4. Some of the wave mode theory of [26] is also presented, this will be used in deriving transfer functions in later chapters. In Chapter 3, the approach to modelling is presented, and parallels will be drawn with existing wave approaches. Both a computational approach based on the calculation of the complex cepstrum, and a simpler approach based on smoothing the transfer function are presented. The formulation of the control problem appears in Chapter 4. The unconstrained problem is solved first, with no requirement that the solution be causal. The solution to the

causal problem is solved by representing it as an $\mathcal{H}_\infty$ control problem, and state-space methods are given to obtain this representation. Chapter 5 demonstrates the approach for several examples. Experimental results on a 24 foot brass beam are presented in Chapter 6. These are compared with previous experimental results using rate feedback and $\mathcal{H}_2$ optimal wave control on the same structure in [29]. Finally, Chapter 7 presents the main conclusions and contributions of the thesis, and discusses a number of possible extensions to this research.

Chapter 2

Mathematical Preliminaries

In Chapter 4, the $\mathcal{H}_\infty$ control design approach will be required, as will a number of results on state space spectral factorizations. Some elements of wave mode theory will also be useful in deriving open and closed loop transfer functions in the examples in Chapter 5. In the interest of simplifying the later discussions, the necessary mathematical background will be presented here.

2.1 $\mathcal{H}_\infty$ Control

A good reference for $\mathcal{H}_\infty$ theory is Francis' book [15], from which much of the following material is drawn. Before discussing the $\mathcal{H}_\infty$ control design method, a number of definitions are required. First, define the Hardy space $\mathcal{H}_\infty$:

Definition 1 *$\mathcal{H}_\infty$ is the space of all complex functions of a complex variable which are analytic and bounded in the open right half plane.*

Thus, $G(s) \in \mathcal{H}_\infty$ if $G(s)$ is both stable and proper. (Though it need not be strictly proper.)

Definition 2 *The norm $\|\cdot\|_\infty$ on $\mathcal{H}_\infty$ is given in the scalar case by*

$$\|G(s)\|_\infty = \sup_{\mathrm{Re}(s)>0} |G(s)| \tag{2.1}$$

Thus, the infinity norm is the supremum of a function in the right half plane. In the matrix function case, the infinity norm is the supremum of the largest singular value of the matrix. From the maximum modulus theorem, it can be shown that any function analytic and bounded in some region achieves its maximum over that region on the boundary, thus

$$\|G(s)\|_\infty = \sup_{\omega\in\mathcal{R}} |G(j\omega)| \tag{2.2}$$

Furthermore, if we consider G to be an operator acting on some (in general, vector) variable x, then the norm of G can be written as an induced operator norm as

$$\|G(s)\|_\infty = \sup_{x\in\mathcal{H}_\infty} \frac{\|Gx\|_2}{\|x\|_2} \tag{2.3}$$

$$= \sup_{\substack{x\in\mathcal{H}_\infty \\ \|x\|_2=1}} \|Gx\|_2 \tag{2.4}$$

This defines the infinity norm in terms of a norm over $\mathcal{H}_2$, which we have yet to define.

Definition 3 *$\mathcal{H}_2$ is the space of all complex functions of a complex variable which are analytic in the open right half plane, and satisfy*

$$\sup_{\xi>0} \left[\frac{1}{2\pi}\int_{-\infty}^{\infty} Tr\left\{|G(\xi+j\omega)|^2\right\} d\omega\right] < \infty$$

The norm $\|\cdot\|_2$ on $\mathcal{H}_2$ is the square root of the left hand side of the above expression, which can be shown to be equivalent to

$$\|G(s)\|_2 = \left[\frac{1}{2\pi}\int_{-\infty}^{\infty} Tr\left\{|G(j\omega)|^2\right\} d\omega\right]^{1/2} \tag{2.5}$$

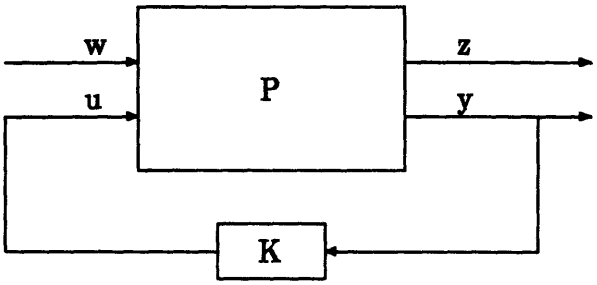

Figure 2.1: Four Block Problem

Further, define *inner* and *outer* functions, using the notation

$$G^{\sim}(s) = G^T(-s) \tag{2.6}$$

Definition 4 *A matrix G in $\mathcal{H}_\infty$ is inner if $G^{\sim}G = I$. G is outer if it has no zeroes in* $\mathrm{Re}(s) > 0$.

Thus an inner function has unit magnitude, is stable, and purely nonminimum phase. An outer function is minimum phase. Note that multiplication by an inner function does not change either the $\mathcal{H}_\infty$ or the $\mathcal{H}_2$ norm of a matrix function.

Now consider the standard four-block control problem, as shown in Figure 2.1. The goal is to find a stabilizing compensator K from the sensed output y to the control input u which will minimize in an appropriate sense the closed loop transfer function from the disturbance w to the controlled variable z. This transfer function is given by the lower linear fractional transformation

$$H(P,K) = P_{wz} + P_{wy}K(I - P_{uy}K)^{-1}P_{uz} \tag{2.7}$$

Note that w contains all disturbance sources, including both process and measurement noise. Similarly, z contains all the quantities to be minimized, including both state and control penalties. In general, the plant P includes the system, actuator and sensor dynamics, and the dynamics of any weighting on w or z.

This representation of the problem is standard in the $\mathcal{H}_\infty$ control formulation. The standard Linear Quadratic Gaussian (or $\mathcal{H}_2$) problem can also be written as the same four block problem, the only distinction being the norm used in the optimization, and the implicit assumptions about the characteristics of the disturbance. In the context of LQG, the disturbance is gaussian white noise, and the $\mathcal{H}_2$-norm of the controlled variable is minimized. If the disturbance can accurately be characterized in this form, then LQG may be the appropriate technique to use. The $\mathcal{H}_\infty$ problem instead minimizes the $\mathcal{H}_\infty$-norm of the transfer function from w to z. From the definition of the operator induced norm Equation (2.4), the appropriate interpretation of the disturbance is the worst case disturbance, having unit power at a single frequency (which corresponds to the maximum amplification of the transfer function). Thus $\mathcal{H}_\infty$ is suited to problems in which the disturbances are likely to have significant narrowband energy at a poorly characterized frequency [6].

Define the notation

$$G(s) = \left[\begin{array}{c|c} A & B \\ \hline C & D \end{array}\right] = C(sI - A)^{-1}B + D \tag{2.8}$$

Hence G can be represented by the finite dimensional system of ordinary differential equations

$$\begin{aligned} \dot{x} &= Ax + Bu \\ y &= Cx + Du \end{aligned} \tag{2.9}$$

Then the four-block transfer function matrix in Figure 2.1 may be represented as

$$P = \left[\begin{array}{c|cc} A & B_1 & B_2 \\ \hline C_1 & D_{11} & D_{12} \\ C_2 & D_{21} & D_{22} \end{array}\right] \tag{2.10}$$

The $\mathcal{H}_\infty$ control problem formulated in this way can be solved using state space methods via an iterative solution to two Riccati equations. These are presented in

[13] with some slightly restrictive assumptions, and in [16] for the general case. The iteration searches for the minimum value of the $\mathcal{H}_\infty$ norm of $H(P,K)$, denoted γ. It is worth noting that at this optimal solution, $H(P,K) = \gamma$ everywhere; the closed loop transfer function is a constant function of frequency.

In addition to the purely LQG solution and the $\mathcal{H}_\infty$ solution to the four-block problem, a combined problem can be studied with a constraint on the $\mathcal{H}_\infty$ performance in an $\mathcal{H}_2$ optimization [6]. This allows a design trade-off between $\mathcal{H}_\infty$ objectives and $\mathcal{H}_2$ objectives, resulting in a compensator that combines the benefits of each. This problem simplifies immensely if the same quantity is penalized in both the $\mathcal{H}_\infty$ and $\mathcal{H}_2$ formulations. In this case, it is equivalent to a maximum entropy problem [31], the solution to which is readily obtainable from the same two Riccati equations as before [30]. In fact, this is equivalent to simply removing the iteration in the $\mathcal{H}_\infty$ solution procedure.

2.2 Spectral Factorization

As is the case for $\mathcal{H}_\infty$ theory, a good reference on spectral factorization is Francis [15], in which the details of the following results are given. The algorithms and theorems will be presented here without proof.

Before proceeding with the definition of a spectral factor and the algorithm for computing it, some additional results from Equation (2.8) are useful. From the definition (2.6) and the expansion in Equation (2.8),

$$G^{\sim}(s) = \left[\begin{array}{c|c} -A^T & -C^T \\ \hline B^T & D^T \end{array}\right] \tag{2.11}$$

The inverse of G can be expressed by writing G in differential equation form (Equation (2.9)), and manipulating to obtain the input as a function of the output,

$$G^{-1}(s) = \left[\begin{array}{c|c} A - BD^{-1}C & BD^{-1} \\ \hline -D^{-1}C & D^{-1} \end{array}\right] \tag{2.12}$$

Of course, this is valid provided $D \neq 0$, so that G^{-1} is proper. For notational purposes, define

$$A^{\times} = A - BD^{-1}C \tag{2.13}$$

Finally, if T is a nonsingular transformation matrix, then

$$\left[\begin{array}{c|c} A & B \\ \hline C & D \end{array}\right] = \left[\begin{array}{c|c} T^{-1}AT & T^{-1}B \\ \hline CT & D \end{array}\right] \tag{2.14}$$

Now, define the spectral factorization of $G(s)$.

Definition 5 *Consider $G(s)$ square with $G^{\sim} = G$, G and G^{-1} proper with no poles on the imaginary axis, and $G(\infty) > 0$. Then G_- is a spectral factor of $G(s)$ if*

$$G = G_-^{\sim} G_- \tag{2.15}$$

and

$$G_-, G_-^{-1} \in \mathcal{H}_\infty \tag{2.16}$$

G_- is a co-spectral factor of G if, instead of the first condition,

$$G = G_- G_-^{\sim} \tag{2.17}$$

with the second condition still holding.

Note that if G_- is a spectral factor of G, then G_-^T is a co-spectral factor of G^T. Thus the same algorithm may be used to compute either the spectral factor, or the co-spectral factor.

From the definition, it is clear that the goal is to split G into two components, one of which is stable and minimum phase, the other of which is anti-stable and purely non-minimum phase. The approach is to find two subspaces, one corresponding to the unstable part of G, and the other corresponding to the stable part of G^{-1}, or the minimum phase part of G. Then if the two spaces are complementary, that is,

they are independent and together span the entire space, then G can be factored into the two desired components.

For G given as in Equation (2.8), the subspace corresponding to the stable part of G is denoted $\mathbf{X}_-(A)$, and that corresponding to the unstable part is $\mathbf{X}_+(A)$. The subspace corresponding to the minimum phase zeroes of G is the same as that corresponding to the left half plane poles of G^{-1}, or $\mathbf{X}_-(A^\times)$.

A transfer matrix $G(s)$ satisfying the conditions in the definition of the spectral factor can be written as

$$G = D + G_1 + G_1^\sim \tag{2.18}$$

where G_1 is stable, minimum phase, and strictly proper. Find a minimal representation of G_1:

$$G_1 = \left[\begin{array}{c|c} A_1 & B_1 \\ \hline C_1 & 0 \end{array}\right] \tag{2.19}$$

Thus from Equations (2.11), (2.18) and (2.19),

$$G = \left[\begin{array}{cc|c} A_1 & 0 & B_1 \\ 0 & -A_1^T & -C_1^T \\ \hline C_1 & B_1^T & D \end{array}\right] \tag{2.20}$$

Since A_1 is stable and $-A_1^T$ is anti-stable,

$$\mathbf{X}_+(A) = \mathrm{Im}\begin{bmatrix} 0 \\ I \end{bmatrix} \tag{2.21}$$

where $\mathrm{Im}(\cdot)$ denotes the image of $(\cdot)$.

At this point, some results about Hamiltonian matrices are required.

Definition 6

$$H = \begin{bmatrix} A & -R \\ -Q & -A^T \end{bmatrix} \tag{2.22}$$

is a Hamiltonian matrix if Q and R are symmetric, and R is either positive semi-definite or negative semi-definite.

The following results all require that H have no eigenvalues on the imaginary axis, and that (A, R) be stabilizable.

If R in Equation (2.22) is zero, then there exists a unique matrix X satisfying the Lyapunov equation

$$A^T X + XA + Q = 0 \tag{2.23}$$

and the modal subspaces of H are given by

$$\mathbf{X}_+(H) = \mathrm{Im}\begin{bmatrix} 0 \\ I \end{bmatrix} \tag{2.24}$$

$$\mathbf{X}_-(H) = \mathrm{Im}\begin{bmatrix} I \\ X \end{bmatrix} \tag{2.25}$$

Note that due to the assumption of (A, R) being stabilizable, this holds only for stable A.

Now consider the case with general R. There exists a unique symmetric matrix X denoted

$$X = Ric\{H\} \tag{2.26}$$

which stabilizes $A - RX$, and satisfies the Riccati equation

$$A^T X + XA + Q - XRX = 0 \tag{2.27}$$

Again,

$$\mathbf{X}_-(H) = \mathrm{Im}\begin{bmatrix} I \\ X \end{bmatrix} \tag{2.28}$$

Furthermore, $\mathbf{X}_-(H)$ and $\mathrm{Im}\begin{bmatrix} 0 \\ I \end{bmatrix}$ are complementary.

Now, return to the spectral factorization problem. The modal subspace $\mathbf{X}_+(A)$ is given by Equation (2.21). It remains to find a representation for $\mathbf{X}_-(A^\times)$, and

show that the two are complementary. However,

$$A^{\times} = \begin{bmatrix} A_1 & 0 \\ 0 & -A_1^T \end{bmatrix} - \begin{bmatrix} B_1 \\ -C_1^T \end{bmatrix} D^{-1} \begin{bmatrix} C_1 & B_1^T \end{bmatrix} \tag{2.29}$$

$$= \begin{bmatrix} A_1 - B_1 D^{-1} C_1 & -B_1 D^{-1} B_1^T \\ C_1^T D^{-1} C_1 & -(A_1 - B_1 D^{-1} C_1) \end{bmatrix} \tag{2.30}$$

is a Hamiltonian matrix. Thus $\mathbf{X}_-(A^{\times})$ is given by Equation (2.28), with

$$X = Ric\left\{A^{\times}\right\} \tag{2.31}$$

and this modal subspace is complementary to $\mathbf{X}_+(A)$.

Defining the transformation matrix

$$T = \begin{bmatrix} I & 0 \\ X & I \end{bmatrix} \tag{2.32}$$

and applying (2.11), then

$$G = \left[\begin{array}{cc|c} A_1 & 0 & B_1 \\ -(C_1 + B_1^T X)^T D^{-1}(C_1 + B_1^T X) & -A_1^T & -(C_1^T + X B_1) \\ \hline C_1 + B_1^T X & B_1^T & D \end{array}\right] \tag{2.33}$$

From this, one can check that

$$G_-(s) = \left[\begin{array}{c|c} A_1 & B_1 \\ \hline D^{-1/2}(C_1 + B_1^T X) & D^{1/2} \end{array}\right] \tag{2.34}$$

satisfies both Equations (2.15) and (2.16).

For $D \neq 0$, the spectral factor of G can be found with this algorithm from the solution to a single Riccati equation. Results also exist for $D = 0$, for example in [42].

2.3 Wave Modelling

This section briefly summarizes a few of the results of Miller [26] that will be used in subsequent chapters.

The partial differential equation (PDE) of a structural member can be transformed into the frequency domain, and written in state space form as

$$\frac{dy}{dx} = A(\omega)y \tag{2.35}$$

where y is a vector of generalized displacements and internal forces at the cross-section x. The eigenvalues of A correspond to wave modes that travel independently. Thus there exists a transformation matrix Y relating the cross-sectional variables y to the wave mode amplitudes w. Since these wave modes travel independently, there exists a diagonal transmission matrix ξ relating the wave mode amplitudes at one position x_1 to those at another. Thus

$$w(x_2, \omega) = \xi(x_2, x_1, \omega)w(x_1, \omega) \tag{2.36}$$

At a junction, such as a boundary where actuator forces act, the wave modes can be split into incoming (w_i) and outgoing (w_o) elements. Partitioning y into displacements u and forces f, then the transformation Y at a junction can be written as

$$\begin{bmatrix} u \\ f \end{bmatrix} = \begin{bmatrix} Y_{ui} & Y_{uo} \\ Y_{fi} & Y_{fo} \end{bmatrix} \begin{bmatrix} w_i \\ w_o \end{bmatrix} \tag{2.37}$$

The boundary condition at the junction relates the displacements u and internal forces f to externally applied forces Q. This can be written as

$$\begin{bmatrix} B_u & B_f \end{bmatrix} \begin{bmatrix} u \\ f \end{bmatrix} = Q \tag{2.38}$$

Using these two equations, the outgoing wave mode amplitudes w_o can be expressed in terms of the incoming wave mode amplitudes w_i and the forces Q:

$$w_o = Sw_i + \Psi Q \tag{2.39}$$

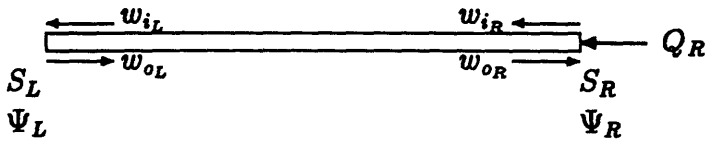

Figure 2.2: One Dimensional Waveguide

S is the open-loop scattering matrix, relating the outgoing waves to the incoming waves. Ψ describes how applied forces Q create outgoing waves. In terms of the previously defined matrices in Equations (2.37) and (2.38),

$$S = -[B_u Y_{uo} + B_f Y_{fo}]^{-1} [B_u Y_{ui} + B_f Y_{fi}] \tag{2.40}$$

$$\Psi = [B_u Y_{uo} + B_f Y_{fo}]^{-1} \tag{2.41}$$

Now consider a closed-loop structure, with feedback from the cross-sectional displacements u to the applied forces Q of the form

$$Q = Ku \tag{2.42}$$

Then the closed-loop scattering matrix can be shown to be

$$S_{CL} = [I - \Psi K Y_{uo}]^{-1} [S + \Psi K Y_{ui}] \tag{2.43}$$

The closed-loop transfer functions of a structural waveguide can also be calculated with this wave approach, using a phase closure algorithm. Consider a simple one-dimensional structure as shown in Figure 2.2. To find the transfer function between applied forces Q at one end (say, for example, the right end), and the generalized displacements y at this end, one would proceed as follows:

$$w_{o_L} = S_L w_{i_L} \tag{2.44}$$

$$w_{o_R} = S_R w_{i_R} + \Psi_R Q_R \tag{2.45}$$

$$w_{i_L} = \xi w_{o_L} \tag{2.46}$$

$$w_{i_R} = \xi w_{o_L} \tag{2.47}$$

where ξ is the transmission matrix from one end of this structure to the other. Combining these equations yields

$$w_{i_R} = \xi S_L \xi w_{o_R} \tag{2.48}$$

$$w_{o_R} = (I - S_R \xi S_L \xi)^{-1} \Psi_R Q_R \tag{2.49}$$

So finally, the relationship between the displacements u and the forces Q is

$$u = (Y_{uo} + Y_{ui} \xi S_L \xi)(I - S_R \xi S_L \xi)^{-1} \Psi_R Q_R \tag{2.50}$$

A minor extension of this result that can be useful but that does not appear in [26] is to calculate the envelope of possible transfer functions in Equation (2.50) for unknown lengths. This corresponds to maximizing or minimizing Equation (2.50) with respect to the length parameter in ξ. For simple structures, such as a uniform beam, this is not difficult, but in general the result is too complicated to be of much value.

As an example of the theory presented in this section, consider a uniform free-free Bernoulli-Euler beam, with bending stiffness EI, and mass per unit length ρA. The PDE for this structure is

$$EI \frac{\partial^4 v}{\partial x^4} + \rho A \frac{\partial^2 v}{\partial t^2} = 0 \tag{2.51}$$

Define the wave number k by

$$k = \sqrt[4]{\frac{\rho A}{EI}} \sqrt{\omega} = c_0 \sqrt{\omega} \tag{2.52}$$

The transformation from cross-sectional to wave mode variables is given by

$$y = \left[\begin{array}{c} v \\ v' \\ \hline -EIv''' \\ EIv'' \end{array}\right] = \left[\begin{array}{cc|cc} 1 & 1 & 1 & 1 \\ jk & k & -jk & -k \\ \hline jEIk^3 & -EIk^3 & -jEIk^3 & EIk^3 \\ -EIk^2 & EIk^2 & -EIk^2 & EIk^2 \end{array}\right] w \tag{2.53}$$

where the partitions indicated correspond to those of Equation (2.37). v and v' are the deflection and slope of the beam at the boundary, respectively, and $-EIv'''$ and EIv'' are the internal shear force and moment, respectively. The wave modes consist of a leftward and rightward travelling wave, and left and right evanescent waves that do not oscillate spatially, but decay with distance. The transmission matrix ξ is

$$\xi = \begin{bmatrix} e^{-ik\ell} & 0 \\ 0 & e^{-k\ell} \end{bmatrix} \tag{2.54}$$

The boundary condition of a free end is specified by

$$\left[\begin{array}{cc|cc} 0 & 0 & -1 & 0 \\ 0 & 0 & 0 & -1 \end{array}\right] \begin{bmatrix} u \\ f \end{bmatrix} = \begin{bmatrix} F \\ M \end{bmatrix} \tag{2.55}$$

where F and M are the externally applied moment and force. These are assumed to act in the same direction as the deflections v and v', so that a positive product of F and v, and of M and v', results in a positive power flow into the beam. Equations (2.40) and (2.41) give the open loop scattering and wave generation matrices as

$$S = \begin{bmatrix} -j & 1+j \\ 1-j & j \end{bmatrix} \tag{2.56}$$

$$\Psi = -\frac{1+j}{2EIk^3} \begin{bmatrix} 1 & k \\ 1 & -jk \end{bmatrix} \tag{2.57}$$

Open and closed loop transfer functions for the beam can then be calculated from Equations (2.43) and (2.50).

Chapter 3

Modelling

The intent of this chapter is to develop a useful model for control design for uncertain modally dense systems. It has been pointed out [19,41] that modes are not useful in this case. The modal frequencies and mode shapes are extremely sensitive to small parameter variations, and are particularly sensitive if the modes are closely spaced. Therefore, much of the information contained in a modal model is often incorrect. This then leads to a difficulty in modelling the uncertainty in a useful, and not overly conservative manner. The modal model also leads to large dimension systems, and an associated computational burden.

The detailed information in a modal model may also be unimportant. While knowledge of the exact mode shapes and frequencies may not be available, this does not imply that nothing is known about the structure, or that nothing can be done to control it. A reasonable control system can be designed without relying on this information. Recognizing this, and recognizing the difficulties associated with a modal approach, a modelling technique is desired which uses a simplified model of the structure, containing only the information that can be accurately determined.

3.1 Dereverberated Mobility Model

The following discussion is restricted to the case where a sensor and actuator are collocated. When this model is ultimately used for control design, this will of course result in suboptimal compensators, since each actuator will only have feedback from a collocated sensor. However, under the assumption of significant uncertainty, while some information about the behavior of the structure can still be determined at the driving point, there is very little information that can be relied upon about the behavior between an actuator and sensor which are separated by many wavelengths of the disturbance. This restriction is therefore reasonable for the control of higher frequency modes, or low authority control. If desired, the low frequency modes which can be well modelled could then be controlled with a high authority control in a HAC/LAC architecture. In this approach, then, a multi-input multi-output structure with actuator and sensor pairs at different locations would be modelled as several separate, single-input single-output systems. Each of these would have collocated actuators and sensors, and the modelling and control design for each of them would be performed independently.

Several approaches other than modal analysis have been used in the past to model structures with significant uncertainty. Statistical Energy Analysis, or SEA [21], is a field which has seen much research, for example in the analysis of machinery vibration. The response of individual modes to the driving noise is not calculated, and only the average response is used. The structure is split into subsystems, and the average energy in each of these subsystems is calculated from coupling factors between them, loss factors within each of them, and the power flow into each subsystem from the driving noise. The result is a description of the structure that includes information about the average energy distribution, and where power is being dissipated. As its name suggests, though, SEA is an analysis tool, and the resulting model is not directly applicable for control design.

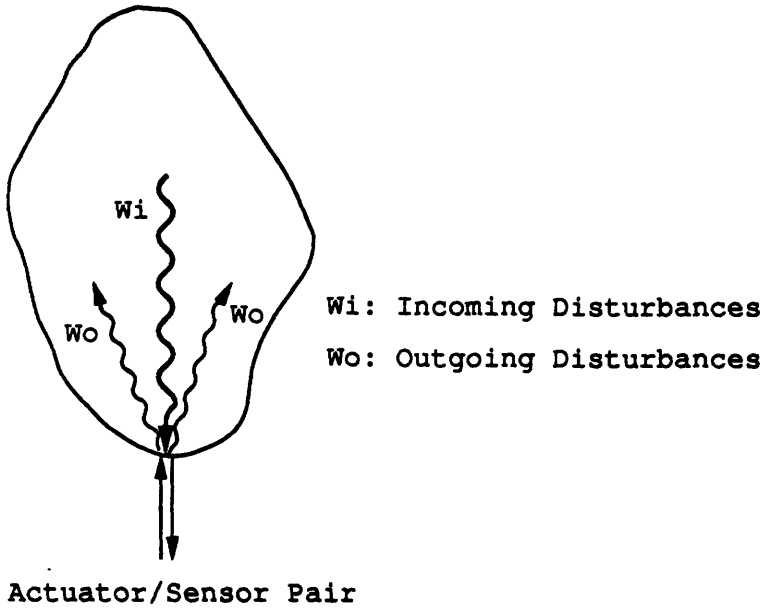

Figure 3.1: Wave behavior in an arbitrary structure

Wave-based models have been used not just for the analysis of structures, but as a basis for control design as well [17,23,28,29,32,33,35,39,40,41]. Here, a local model based on the partial differential equation (PDE) that applies to the structural member at the point in question is developed. The wave model contains the same information as the PDE, however, depending on the control design approach, there may be other implicit assumptions that introduce problems, such as ignoring the effect of boundary conditions at other points of the member on the local response. In most studies, the structural members have been simple one dimensional waveguides, and the structures analyzed have been restricted to those that could be well represented by networks of such waveguides. It may be difficult, however, to obtain a wave description for many complicated structures, because not all structures can be well represented in this manner.

For some arbitrary structure, as shown in Figure 3.1, insight into the nature of the problem can still be obtained from a wave approach. Various disturbances are created at certain points in the structure and propagate through it. At any point in

the structure, such as at an actuator, the disturbance will be scattered. In general, each of the resulting outgoing disturbances will eventually affect any global cost criterion. Thus without a detailed and accurate description of how each outgoing wave propagates, the goal of the control system should be to minimize the energy of each of these disturbances. Since the scattering behavior is a function of only the local dynamics, this goal can be achieved with only a local model of the structure.

An alternative approach to waves for obtaining such a model is to represent the structure by its dereverberated driving point mobility [22]. The mobility is the ratio of a generalized velocity and a generalized force, or the inverse of the mechanical impedance [14]. It is the transfer function between two variables whose product is the power flow into the structure, thus the sensors and actuators must be both collocated and dual. The response at a point can be considered to be the sum of two parts: a *direct field*, due to the local dynamics; and a *reverberant field*, which is caused by energy reflected back from other parts of the structure. The term "dereverberated" implies that the "reverberant" part of the response has been removed before computing the mobility. It should be possible to model the direct field more easily and accurately than the reverberant field, as it depends only on a few parameters, while the reverberent field depends on the entire structure. For the same reason, it is the reverberant field that contains greater detail, and requires more degrees of freedom to model. Thus by using the dereverberated mobility, a lower order model can be used that is based only on the details of the structure which can be accurately modelled.

3.2 Cepstral Analysis Approach

The dereverberated mobility may be calculated through the use of the cepstrum [22] of the impulse response. The cepstrum is the inverse Fourier transform of the log of the complex spectrum, and is a function of time. For the impulse response

$y(t)$, the complex spectrum is given by

$$Y(\omega) = \int_0^\infty y(t)e^{-j\omega t}\mathrm{dt} \tag{3.1}$$

Since a structural system is causal, $y(t)$ should be 0 for $t < 0$. Also,

$$\log Y = \log|Y| + j\phi_y \tag{3.2}$$

where the log magnitude is an even function of frequency, and the phase ϕ_y is an odd function. The complex cepstrum is given by

$$C_y(t) = \mathcal{F}^{-1}(\log Y) \tag{3.3}$$

$$= \mathcal{F}^{-1}(\log|Y|) + \mathcal{F}^{-1}(j\phi_y) \tag{3.4}$$

and is purely real. The inverse Fourier transform is given by

$$\mathcal{F}^{-1}(Y(\omega)) = \frac{1}{2\pi}\int_{-\infty}^{\infty} Y(\omega)e^{j\omega t}\mathrm{d}\omega \tag{3.5}$$

The low time portion of the cepstrum corresponds to the direct response, and the high time portions correspond to the reverberant response, with spikes at times corresponding to the return times of the impulse from the rest of the structure. Windowing the cepstrum before the first of these yields the direct response, which can then be transformed back to the frequency domain to yield the dereverberated impulse response.

The truncation time to choose can be based on the level of confidence in the impulse response data. This illustrates one of the differences between the dereverberated mobility and a local wave model, that being direct control over how much of the structure is included in the model. By truncating the cepstrum at the appropriate point, some information about the rest of the structure is maintained while the details of it are ignored. Thus the control design is provided with more information, allowing it to generate a better controller.

The fundamental distinction between this and wave approaches is the ability to treat generic structures without having to represent them with a wave model. While the concept of direct and reverberant fields is based on wave ideas, there is no requirement to actually identify a local wave model. All that is needed is the input/output behavior at the driving point, which may be found from experimental data, calculated from some nominal model, or found analytically, perhaps even from a wave model. This approach is shown schematically in Figure 3.2 for the transfer function from force to collocated velocity at one end of a free-free beam.

This structure provides an interesting example, since the dereverberated mobility can also be found directly from the wave approach described in Section 2.3. The reverberant field is created by reflections from the far end of the beam, so if the scattering matrix for this end is set to zero, the dereverberated mobility can be calculated from Equation (2.50). The result is

$$\frac{\dot{y}}{F} = \frac{\sqrt{2}}{(\rho A)^{3/4}(EI)^{1/4}} \cdot \frac{1}{\sqrt{s}} \tag{3.6}$$

This can be scaled so that the transfer function is just

$$\frac{\dot{y}}{F} = \frac{1}{\sqrt{s}} \tag{3.7}$$

The cepstrum for both the true and dereverberated structures can also be calculated from theory:

$$C_{y_{true}} = \mathcal{F}^{-1}\left\{ \log \frac{\prod_{i=1}^{\infty}(s - z_i)}{\prod_{i=1}^{\infty}(s - p_i)} \right\} \tag{3.8}$$

$$= \begin{cases} \frac{2}{t}\left(\sum_{i=1}^{\infty} e^{-\zeta_{p_i}\omega_{p_i}t}\cos(\omega_{p_i}t) - \sum_{i=1}^{\infty} e^{-\zeta_{z_i}\omega_{z_i}t}\cos(\omega_{z_i}t)\right) & t > 0 \\ 0 & t \leq 0 \end{cases} \tag{3.9}$$

$$C_{y_{derev}} = \mathcal{F}^{-1}\left\{ \log \frac{1}{\sqrt{j\omega}} \right\} \tag{3.10}$$

$$= \begin{cases} \frac{1}{2t} & t > 0 \\ 0 & t \leq 0 \end{cases} \tag{3.11}$$

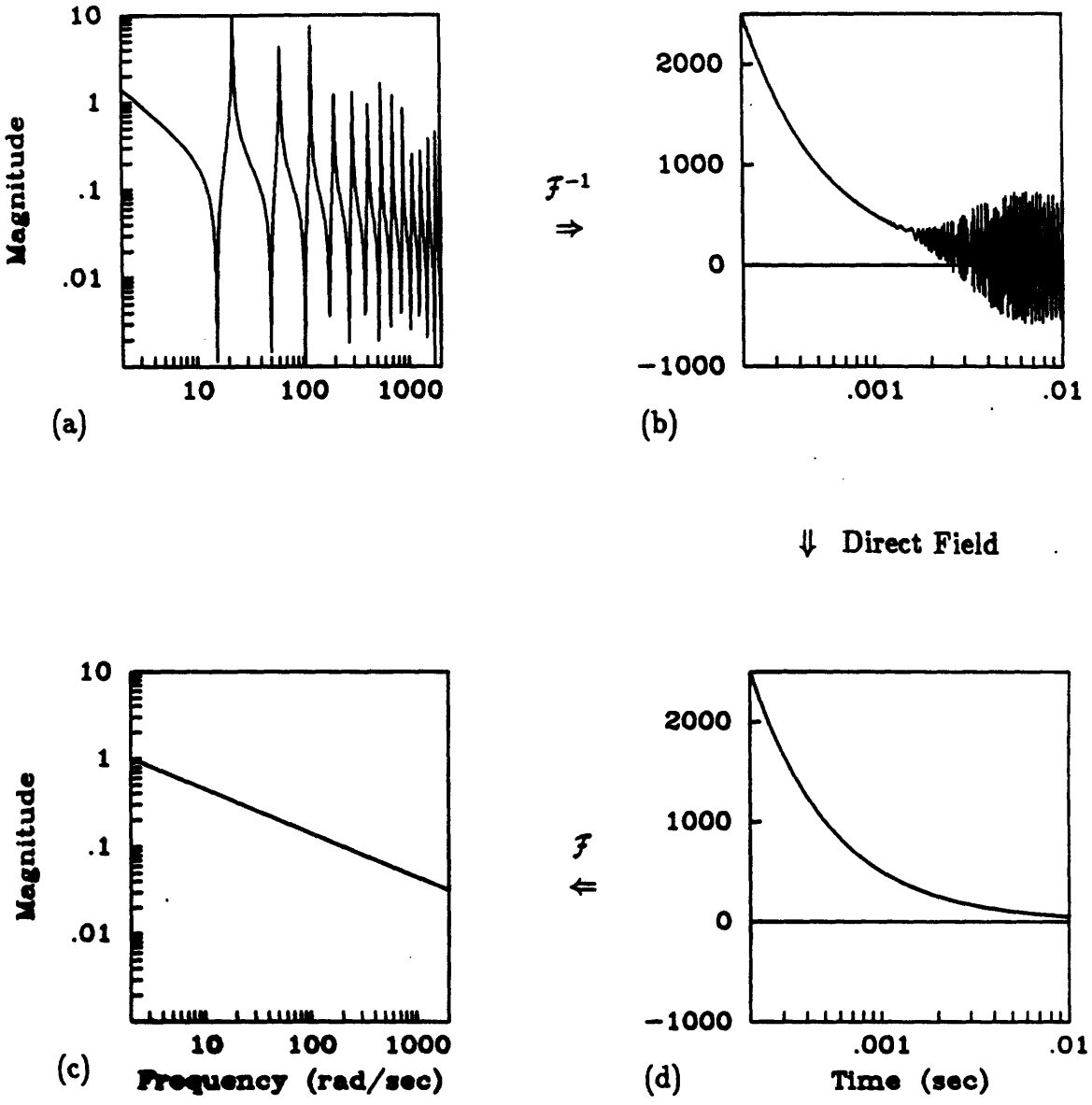

Figure 3.2: Calculation of dereverberated mobility from complex cepstrum. Transfer function (a) and cepstrum (b) of a free-free beam, dereverberated cepstrum (c) and dereverberated transfer function (d).

The sum in Equation (3.9) is over all poles $p_i = \varsigma_{p_i}\omega_{p_i} + j\omega_{p_i}$ and zeroes $z_i = \varsigma_{z_i}\omega_{z_i} + j\omega_{z_i}$.

These are the functions plotted in Figure 3.2. It should be emphasized that this theoretical approach would *never* be used in practice to compute the cepstrum. It does, however, provide a validation of the approach. The correct dereverberated mobility cannot be found exactly by simply truncating the cepstrum of the reverberant structure in Figure 3.2(b) to obtain the dereverberated cepstrum in Figure 3.2(c). If straight truncation were used, though, the resulting dereverberated mobility would be the convolution of Figure 3.2(d) with a *sinc* function, and this would not differ significantly from the desired function in the region of interest.

Further details on the calculation of the cepstrum, and its use in removing reverberation can be found in [9,38]. In general, however, it is not necessary to go through the procedure of computing the cepstrum, truncating it, and transforming back to the frequency domain.

3.3 Smoothing Approach

There is an alternative, less accurate, but much simpler way to calculate the dereverberated mobility. This is based on the observation that the effect of ignoring the reverberant field is to smooth out the transfer function. If no energy returns from beyond some closed surface surrounding the actuator, then this is equivalent to the structure beyond this surface either being infinite in extent, or having perfectly absorbing boundary conditions. This has also been shown [19,36] to be equivalent to the logarithmic mean of the original transfer function.

Hodges and Woodhouse [19] demonstrate this by showing that the assumptions that lead to using the smoothed transfer function in place of the original transfer function also lead to using a dereverberated model in place of the original reverberant system, and that these two new systems are equivalent. This is shown by consid-

ering the mean power input to a system by an excitation source with a broadband spectrum, and comparing the modal interpretation with the wave interpretation.

Skudrzyk [36] considers the transfer function of a reverberant system, and the affect of damping. As damping is added, the maxima of the transfer function decrease, and the minima increase. Eventually the transfer function is a smooth curve at the average of these maxima and minima. This response curve is therefore that that would be obtained if the system were sufficiently damped and sufficiently large, so that the reflected waves do not contribute significantly to the response. The dereverberated system is therefore obtained by increasing the damping and size of the system, and has a transfer function which is the logarithmic mean of the original transfer function. This response curve corresponds to the amplitude of the direct field that is generated by the input.

Thus another way to compute the dereverberated mobility is simply to take a logarithmic average of the magnitude of the transfer function. This is not surprising, considering that the cepstral analysis approach described earlier is essentially the same as low-pass filtering the logarithmic frequency response. The phase can be determined uniquely from Bode's Gain-Phase Theorem [8], using the fact that the dereverberated mobility is positive real. In practice, this method should be adequate. Fitting the result with a rational polynomial gives a model that captures the essential dynamics of the system over a wide frequency range that encompasses many modes, with only a small number of poles and zeroes.

Figure 3.3(a) and (b) shows the transfer function of a free-free Bernoulli-Euler beam. Rather than evaluating the system response only on the $j\omega$ axis, however, the transfer function is plotted for part of the right half complex plane; that is, as a function of both the real and imaginary parts of the Laplace transform variable s. The familiar sharp peaks and valleys associated with lightly damped structures only appear near the imaginary axis. Farther away from the axis, the effect of individual modes is smeared out, and the transfer function becomes smooth. Since the dere-

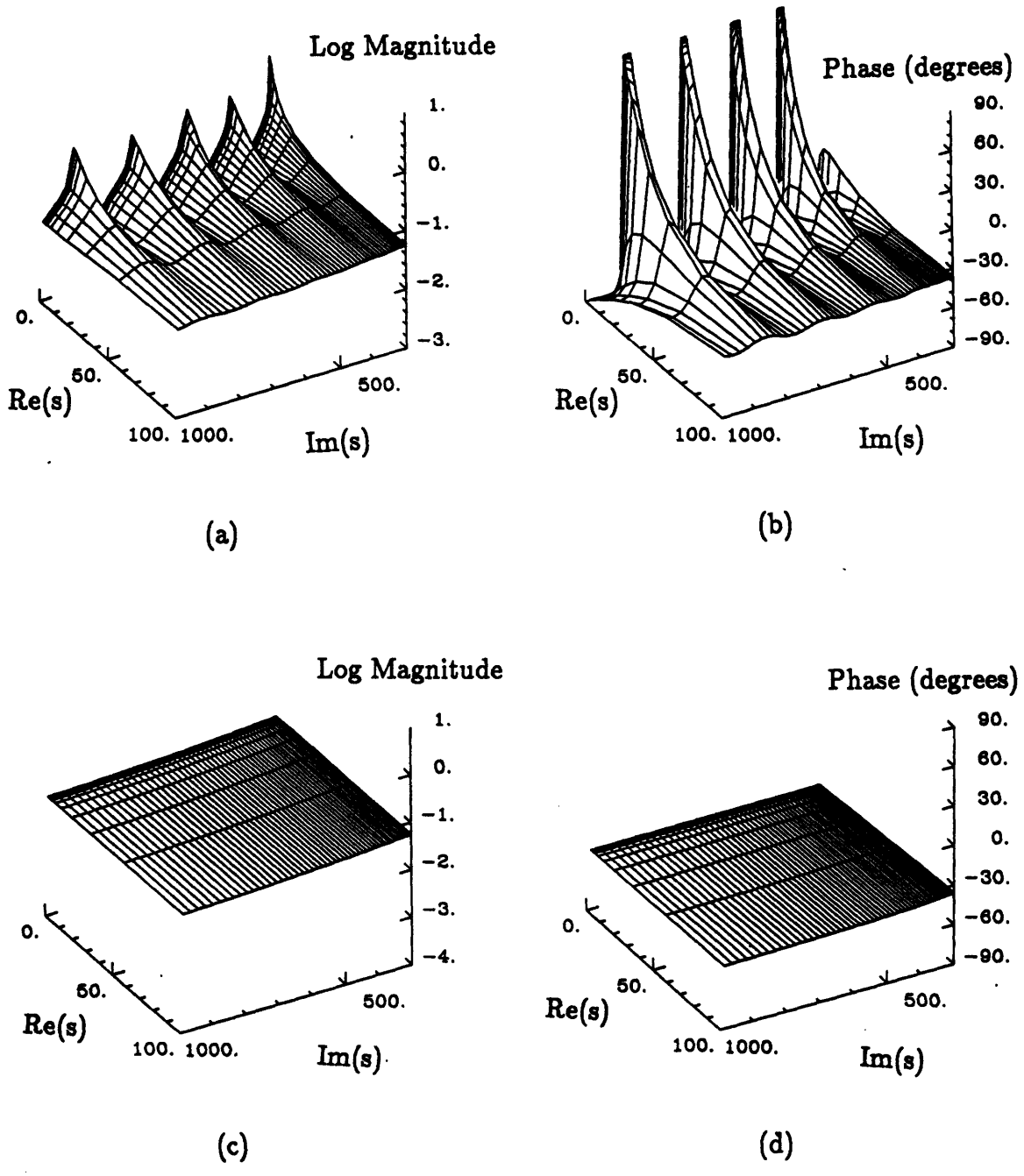

Figure 3.3: Transfer function of a beam evaluated as a function of both the real and imaginary parts of the complex Laplace variable: magnitude (a) and phase (b) of a finite beam, and magnitude (c) and phase (d) of the dereverberated beam.

verberated system can be obtained from the original system by adding damping, as noted earlier, it is the dereverberated mobility to which the transfer function approaches as the real part of the Laplace variable increases. Therefore, if the goal of the control system is to move the poles away from the axis, this smooth transfer function should be a good approximation to the structure. The significance of this figure for control design will be discussed further in Chapter 4. Figure 3.3(c) and (d) shows the dereverberated transfer function for the same system. The dereverberated mobility is a good approximation to the structure everywhere except near the $j\omega$ axis.

As an example of the dereverberated mobility approach on a modally dense structure, consider the transfer functions plotted in Figure 3.4. The graph shows an experimental transfer function measured from endpoint moment to endpoint slope rate on a pinned-free brass beam suspended in the laboratory at M.I.T. (This beam is discussed in more detail in Chapter 6.) Note the high modal density above a few tens of hertz; it seems reasonable that a control design that relied upon the exact location of each mode would be undesirable. The average amplitude, however does not depend at all on the length of the beam or the nature of the boundary condition at the far end. Also plotted in the figure is the theoretical response of a semi-infinite Bernoulli-Euler beam (the straight line, calculated again from the wave approach of Section 2.3), and the average response, which differs from the Bernoulli-Euler prediction only at low and high frequencies. It is this average response that would be the appropriate dereverberated admittance, though the straight line approximation would probably be adequate if the central frequency range is the range of interest.

The dereverberated mobility model is not intended to accurately represent the structure; it clearly fails in this regard. However, it is hoped that this will be a useful model for the design of control systems for the structure. While the resonant and anti-resonant details of the full reverberant mobility are not explicitly modelled,

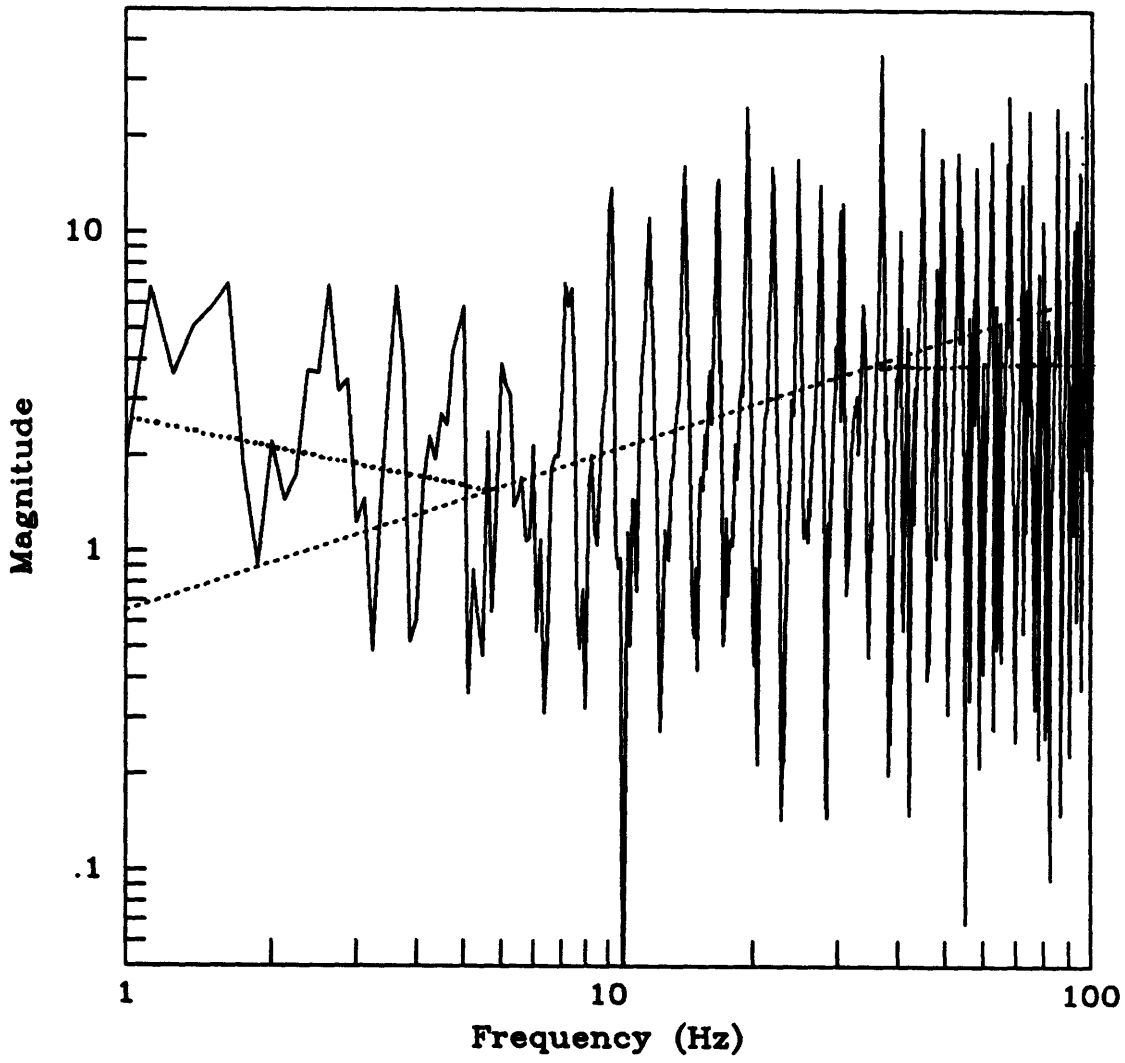

Figure 3.4: Example of dereverberation: experimental transfer function (solid), theoretical semi-infinite transfer function (dashed) and dereverberated mobility (dotted).

the reverberant field is composed of waves whose behavior is governed by the local dynamics of the controlled junction each time they pass through it. Thus if the local dynamics can be appropriately modified based on a local model, then the complete reverberant field can be controlled.

Chapter 4

Control Design

The previous chapter described the modelling approach used, while this chapter focuses on the design of the control system for this model. There are two main objectives to be satisfied by the control design. It must be guaranteed to be stabilizing for all possible plants, and it must provide good performance, again for all possible plants. In order to guarantee stability, positive real feedback from velocity to force will be required. One could, for example, select rate feedback, which is guaranteed to be stable, but this does not necessarily give the best performance that could be achieved. Velocity feedback is only one possible choice of positive real feedback; the object of this chapter is to derive the optimal positive real compensator.

The criterion to be used for optimality will be the minimum power flow into the structure. That is, power extracted from the structure will be maximized. Power flow is the appropriate quantity to minimize to provide active damping of the structure, and allows a guarantee of stability by ensuring that the power flowing into the structure due to the control is always negative.

Miller *et al.* [28] minimized the $\mathcal{H}_2$ norm of the power flow. This required some assumptions about the power spectral density of the disturbance entering the junction. In the actual structure, this is related to the control through the disturbance that previously departed the junction. In the wave model, however, it was assumed

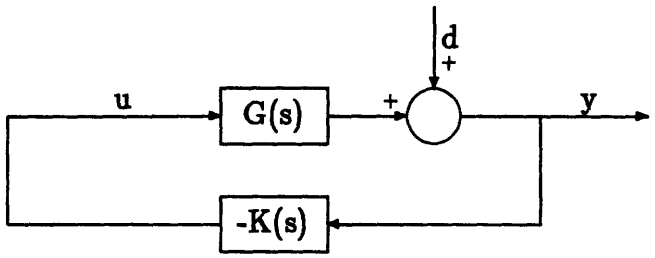

Figure 4.1: System Block Diagram I

constant and independent of the control. As a result, in general the compensators obtained allowed power to be added at some frequencies, since this behaviour could not destabilize the design model. This problem can be avoided by minimizing the power flow in an $\mathcal{H}_\infty$ setting. For an open-loop system, the power removed by the controller is zero. If the closed loop power flow is guaranteed to be no worse at all frequencies, then the closed loop system is guaranteed to be stable. In fact, it is sufficient to place a constraint on the maximum value of the power flow which guarantees it to be negative at all frequeucies. An $\mathcal{H}_2$ optimization [6] can then be used, which may improve the overall performance.

Define $G(s)$ to be the dereverberated driving point mobility, and assume some disturbance input d to be additive at the output. Then the output y is related to the input u and the disturbance via

$$y(s) = G(s)u(s) + d(s) \tag{4.1}$$

as shown in Figure 4.1. As yet, no assumptions have been made about the nature of the disturbance.

Recall that in Chapter 2 the noise assumptions made in $\mathcal{H}_\infty$ and $\mathcal{H}_2$ optimizations were discussed. Now consider this in the context of the model defined in Chapter 3. The disturbance d in Equation (4.1) can be thought of as originating from two sources: the original disturbance input to the real structure, and the reverberant field ignored in the modelling process. This second source will have significant

power at the modal frequencies, and if the closed loop damping is still relatively small, then in steady state this will be much larger than the physical disturbance. Thus the disturbance spectrum in Equation (4.1) consists of significant power in narrowband but unknown frequency ranges, which are exactly the assumptions indicated in Chapter 2 as being appropriate for $\mathcal{H}_\infty$ minimization.

4.1 Unconstrained Optimum

Before finding a compensator which minimizes the worst case power flow, consider finding the compensator which minimizes the power flow at each value of the Laplace transform variable s. The control law is of the form

$$u = -Ky \tag{4.2}$$

where the explicit dependence on the Laplace transform variable has been dropped. Solving for the control in terms of the disturbance from Equation (4.1) gives

$$u = -(I + KG)^{-1}Kd \tag{4.3}$$

$$= Hd \tag{4.4}$$

Then the output can also be represented in terms of the disturbance as

$$y = (I + GH)d \tag{4.5}$$

The instantaneous power flow into the structure is the product of the input $u(t)$ and the output $y(t)$, since $G(s)$ is an mobility. The average power flow can be expressed as a time integral of the instantaneous power flow [27],

$$\mathrm{P}_{ave} = \lim_{T\to\infty} \frac{1}{2T} \int_{-T}^{T} y^T(t)u(t)\mathrm{d}t \tag{4.6}$$

Making use of Parseval's theorem, this can be transformed into the frequency domain:

$$\mathrm{P}_{ave} = \frac{1}{2} \int_{-\infty}^{\infty} \left(u^H(j\omega)y(j\omega) + y^H(j\omega)u(j\omega)\right) \frac{\mathrm{d}\omega}{2\pi} \tag{4.7}$$

The integrand of the right hand side of Equation (4.7) represents the steady state, or average, power flow into the structure as a function of frequency [27]. For convenience, the average power flow at each frequency can be defined without the factor of $\frac{1}{2}$, as

$$\mathcal{P}(\omega) = u^H(j\omega)y(j\omega) + y^H(j\omega)u(j\omega) \tag{4.8}$$

where $(\cdot)^H$ indicates Hermitian, or complex conjugate transpose. The Hermitian operator is not analytic in the complex plane. Instead, the appropriate operator is the analytic continuation of the conjugate from the $j\omega$ axis to the remainder of the plane. This operator is denoted $(\cdot)^\sim$ and is defined as in Chapter 2 as

$$F^\sim(s) = F^T(-s) \tag{4.9}$$

Substituting the earlier expressions for u and y into Equation (4.8) yields

$$\mathcal{P}(\omega) = d^\sim \{H^\sim(I + GH) + (I + GH)^\sim H\} d \tag{4.10}$$

This equation gives the power flow into the structure as a function of the compensator. The optimal value of H is that which minimizes the expected value of this expression at each point in the complex plane. Since the power flow is a scalar, it is equal to its trace. So

$$\begin{aligned} \text{Cost}(s) &= \mathrm{E}\left[\text{Trace}\{dd^\sim [H^\sim(I + GH) + (I + GH)^\sim H]\}\right] && (4.11) \\ &= \text{Trace}\{\Phi_{dd}[H^\sim(I + GH) + (I + GH)^\sim H]\} && (4.12) \end{aligned}$$

where $\Phi_{dd} = \Phi_{dd}^T = \mathrm{E}[dd^\sim]$ is the power spectral density of the disturbance d.

Making use of the symmetry in (4.12) gives that at the optimum,

$$H^\sim = H \tag{4.13}$$

Using this result, then differentiation gives

$$\frac{\partial(\text{Cost})}{\partial H} = 2\Phi_{dd} + \Phi_{dd}H(G + G^\sim) + (G + G^\sim)H\Phi_{dd} = 0 \tag{4.14}$$

From this equation, the optimal H is given by

$$H_{opt} = -(G + G^{\sim})^{-1} \tag{4.15}$$

provided this inverse exists. If it does not exist, this implies that if Φ_{dd} is full rank, Equation (4.15) is valid, and an infinite amount of power can be extracted from the structure. If Φ_{dd} is singular, then Equation (4.15) is not valid, however in this case, Equation (4.14) is not sufficient to uniquely determine H. Since in general the approach of this thesis deals with SISO systems, this case is not too significant a restriction on the applicability of this result. Non-scalar Φ_{dd} will only arise if a structure has multiple actuator and sensor pairs of different types at the same location, since if they were at different locations the structure would be modelled and controlled as separate SISO systems.

If the inverse in Equation (4.15) exists, then this compensator is independent of the disturbance spectrum Φ_{dd}. From Equations (4.3) and (4.4), the compensator K is related to H by

$$K = -H(I + GH)^{-1} \tag{4.16}$$

so finally,

$$K_{opt} = (G^{\sim})^{-1} \tag{4.17}$$

This compensator extracts the maximum possible power from the structure at every frequency.

This result is not new; it corresponds to the impedance matching condition found, for example, in [10]. The maximum energy dissipation is obtained if the impedance of the compensator is the complex conjugate of the impedance of the load, which in this case is the rest of the structure.

In general, however, the compensator in Equation (4.17) is noncausal, and cannot be implemented in real time, since it requires knowledge of future information. The dereverberated mobility $G(s)$ must be both stable and causal, and is therefore

right half plane analytic (RHPA). Since it is strictly positive real, it must also be minimum phase, and thus the optimal compensator in Equation (4.17) will be left half plane analytic (LHPA). So every pole of the compensator is in the right half plane. This does not necessarily imply that the compensator is unstable. A right half plane pole corresponds to a unique transfer function, but there are two time domain systems with this transfer function. One is causal and unstable, so that the impulse response is zero for negative time, and increases with increasing positive time. The other is noncausal and stable, with its impulse response zero for positive time, and decreasing to zero as time decreases to minus infinity.

One can determine which of these two systems applies in this case from a Nyquist plot. Since both the compensator and the plant are strictly positive real, there are no encirclements of the point -1, and thus K must be stable for the closed loop system to be stable. This implies that in general, this compensator is noncausal. K can be stable, causal, and LHPA only if it is a constant, and hence only if the dereverberated mobility is a constant. One such case is that of a uniform rod in compression, with a collocated force actuator and velocity sensor at one end. In this case, Equation (4.17) corresponds exactly to the matched termination for the rod.

Some understanding of why the optimal compensator is almost always noncausal can be found from root locus arguments. For a point λ to be on the root locus of the plant $P(s)$, the compensator $K(s)$ must satisfy

$$1 + P(\lambda)K(\lambda) = 0 \tag{4.18}$$

In order to place the structural poles far into the left half plane, the relevant plant $P(s)$ is the structure as it appears from far into the left half plane.

For a lightly damped structure with a large number of closely spaced poles and zeroes, one can divide the complex plane into three regions. Near the $j\omega$ axis, and close to the poles and zeroes, the transfer function varies significantly from its maxima to its minima, and the phase varies between +90° and -90°. If one looks at

the structure from farther into the right half plane, the effect of individual poles and zeroes becomes smeared out, and the transfer function approaches the smoothed, or dereverberated transfer function $G(s)$. The phase of G in some frequency region will be the average phase of the original transfer function near that region, and the magnitude will be the logarithmic mean of the magnitude of the original transfer function near that region. This behaviour is shown graphically in Figure 3.3.

In the left half plane, however, the structure's transfer function is not $G(s)$. To determine the phase contribution of each pole and zero, the contour to consider must now be to the left of every pole and zero, and so each phase change has opposite sign. The result is that in the left half plane, the structural transfer function approaches $-G(-s)$. Therefore, to move the poles far into the left half plane, $K(s)$ must satisfy

$$1 - G(-s)K(s) = 0 \tag{4.19}$$

or

$$K(s) = 1/G(-s) \tag{4.20}$$

as given in Equation (4.17).

If this compensator could be implemented, all of the structural poles could be moved arbitrarily far into the left half plane. Instead, the best causal compensator must be found.

4.2 Causal Optimum

The wave model of Miller *et al.* [28] can also be put in a form similar to that of Equation (4.1), though only for structures composed of waveguides. As discussed earlier, Miller *et al.* performed an $\mathcal{H}_2$ optimization of the power flow, which did not guarantee dissipation at all frequencies, and thus did not guarantee closed loop stability. A more appropriate optimization to guarantee stability is to minimize the worst case power dissipation, hence a minimax optimization of the power flow into

the structure. As will be shown shortly, this can be cast as an $\mathcal{H}_\infty$ minimization problem. In order for this to make sense, though, the disturbance input d should be normalized to provide the same amount of power available to be dissipated at each frequency. This provides the designer with complete control over the relative importance of one frequency range to another, by removing any inherent frequency weighting from the problem.

With the optimal noncausal compensator derived in the previous section, Equation (4.17), the closed loop power flow into the structure is given by Equations (4.10) and (4.15) as

$$P = -d^{\sim}(G + G^{\sim})^{-1}d \tag{4.21}$$

Represent the disturbance d as

$$d = G_0 w \tag{4.22}$$

Then if the input w has unit magnitude at a certain frequency, the optimal noncausal compensator will dissipate unit power at this frequency, provided that the transfer function G_0 is the co-spectral factor of $G + G^{\sim}$, given by

$$G_0 G_0^{\sim} = G + G^{\sim} \tag{4.23}$$

The block diagram for this system is shown in Figure 4.2, and the system (Equation (4.1)) becomes

$$y(s) = G(s)u(s) + G_0(s)w(s) \tag{4.24}$$

Now, consider the problem of finding a causal compensator that will minimize the worst case power flow in Equation (4.8). This quantity represents the power flow into the structure, which will hopefully be negative. The goal is to find a compensator K that results in

$$\min_{u} \max_{w} \left\{ u^H(j\omega)y(j\omega) + y^H(j\omega)u(j\omega) \right\} \tag{4.25}$$

This minimax problem can be solved directly, using the approach of [34]. Alternatively, it can be reformulated as an $\mathcal{H}_\infty$ problem, for which software to find K

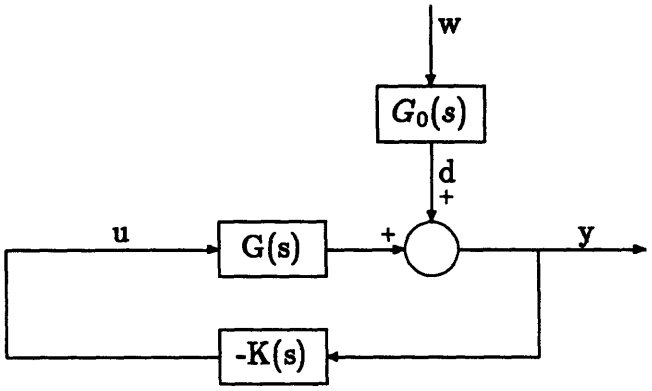

Figure 4.2: System Block Diagram II

exists. In order to cast this as an $\mathcal{H}_\infty$ optimization, however, the performance index must be positive definite. Note, though, that the best causal compensator can dissipate no more power than the unconstrained, noncausal optimum. Thus if the disturbance power $w^{\sim}w$ is added to the cost, positive definiteness will be assured.

The cost at each frequency is therefore

$$\begin{aligned}
\text{Cost}(\omega) &= w^{\sim}w + u^{\sim}y + y^{\sim}u && (4.26)\\
&= w^{\sim}w + u^{\sim}(Gu + G_0w) + (Gu + G_0w)^{\sim}u && (4.27)\\
&= \begin{Bmatrix} u \\ w \end{Bmatrix}^{\sim} \begin{bmatrix} G + G^{\sim} & G_0 \\ G_0^{\sim} & I \end{bmatrix} \begin{Bmatrix} u \\ w \end{Bmatrix} && (4.28)\\
&= |G_0^{\sim}u + w|^2 && (4.29)
\end{aligned}$$

From this, the relevant output that should be minimized is

$$z = G_0^{\sim}u + w \tag{4.30}$$

Combining this with the system equation (4.24), the result can be written as a four block problem (compare with Figure 2.1):

$$\begin{Bmatrix} z \\ y \end{Bmatrix} = \begin{bmatrix} I & G_0^{\sim} \\ G_0 & G \end{bmatrix} \begin{Bmatrix} w \\ u \end{Bmatrix} \tag{4.31}$$

The compensator from y to u that minimizes the $\mathcal{H}_\infty$ norm of the transfer function from w to z will minimize the maximum power flow into the structure.

For computation, however, the unstable (1,2) block in Equation (4.31) is unacceptable. Any allowable compensator must stabilize this block, while the only important stability constraint is on the output y. Recall from Chapter 2, however, that the norm of z is unchanged by multiplication by an inner function. Define $\Delta(\cdot)$ to be the characteristic polynomial of the transfer function $(\cdot)$, and define the inner function

$$G_1(s) = \frac{\Delta(G_0^{\sim}(s))}{\Delta(G_0(s))} \tag{4.32}$$

Then redefine z to be

$$z = G_1 G_0^{\sim} u + G_1 w \tag{4.33}$$

so that the four-block problem (4.31) becomes

$$\begin{Bmatrix} z \\ y \end{Bmatrix} = \begin{bmatrix} G_1 I & G_1 G_0^{\sim} \\ G_0 & G \end{bmatrix} \begin{Bmatrix} w \\ u \end{Bmatrix} \tag{4.34}$$

which is stable.

In general, it may be desirable to weight some frequency ranges more heavily than others, while still requiring that power be removed at all frequencies. This could be because there is a known disturbance source in a certain range, because structural modes are less well damped within this range, or because the performance requirements put more emphasis on this range. Similarly, there will usually be some frequency beyond which performance is not required, and the weighting can also be chosen to reflect this.

The manner in which the weighting is introduced into the problem must be such that if power is added to the structure somewhere, the resulting cost will be worse than the open-loop cost. Hence, rather than weighting the sum of the disturbance input power and the power input by the control, as in Equation (4.26), define the

cost to be the sum of the disturbance power and some frequency weighted control power, as

$$\text{Cost}(\omega) = w^{\sim}w + W_1^{\sim}(u^{\sim}y + y^{\sim}u)W_1 \tag{4.35}$$

which can be manipulated into the form

$$\text{Cost} = \left| \begin{array}{c} W_1(G_0^{\sim}u + w) \\ W_2 w \end{array} \right|^2 \tag{4.36}$$

where W_1 is the selected frequency weighting, and W_2 is defined by the relationship

$$|W_1|^2 + |W_2|^2 = 1 \tag{4.37}$$

The output z of the four block problem is then

$$z = \left\{ \begin{array}{c} W_1(G_0^{\sim}u + w) \\ W_2 w \end{array} \right\} \tag{4.38}$$

Note that as desired, the open loop cost is unity everywhere, and the cost is greater than unity at any frequency where power is added to the structure. Thus as before, a closed loop cost of less than unity guarantees stability.

The only constraint on W_1 is that its magnitude be less than or equal to unity at all frequencies. Without this constraint, there is no guarantee that the cost be positive definite, and the minimization could fail. Where W_1 is small, a greater amount of control effort is required to reduce the cost than before, and thus there is more power removed. Hence, in order to emphasize some frequency range more heavily, the weighting function W_1 should be chosen to be smaller within that region.

Recall from Chapter 2 that one of the properties of $\mathcal{H}_\infty$ compensators is that at the optimum, the closed loop transfer function being minimized is a constant function of frequency, equal to some number γ [15]. From this, and Equation (4.35), the closed loop power absorbed by the compensator can be related to γ and the weighting function. This is expressed as a fraction of the power absorbed by the

unconstrained optimal compensator:

$$P(\omega) = \frac{1-\gamma^2}{|W_1|^2} \tag{4.39}$$

This provides some insight into how to select W_1.

The cost in Equation (4.26) or (4.35) can also be modified to include a penalty on the control effort, $\rho u^{\sim} u$. The four block problem (4.34) is modified to include an additional output in the vector z, corresponding to $\sqrt{\rho}u$. This allows a trade-off between performance and control, and also guarantees a proper compensator. Similarly, it is straightforward to modify the four block problem (4.34) to include sensor noise. An additional disturbance input is included in the vector w which affects only the sensor output y.

The final result of this approach is a positive real compensator, which is guaranteed to be stabilizing for any positive real plant. However, if there are any time delays, actuator or sensor dynamics, or if the actuator and sensor are not truly collocated and dual, then the structure will not be positive real at all frequencies. Stability can still be guaranteed if the complementary sensitivity is bounded above by the inverse of the difference of the true structure from positivity, as noted by Slater [37].

This constraint can be represented as a constraint on the $\mathcal{H}_\infty$-norm of an appropriate transfer function. If the error bound is given as in Equation (1.3) for the difference from positivity, then stability can be guaranteed if the compensator is positive real and, as in Equation (1.2),

$$\left\| GK(I+GK)^{-1}L_m \right\|_\infty \leq 1 \tag{4.40}$$

The compensator is positive real if power is dissipated at all frequencies, or

$$\|z\|_\infty \leq 1 \tag{4.41}$$

with z being given by Equation (4.30) or (4.38). Thus this problem is one of minimizing the $\mathcal{H}_\infty$ norm of one transfer function (Equation (4.41)), with a constraint on the $\mathcal{H}_\infty$ norm of another transfer function (Equation (4.40)).

4.3 State Space Computation

The calculation of the optimal compensator for the four-block problem is most easily performed in state space, since software exists to solve the state space $\mathcal{H}_\infty$ four-block problem. The first step then is to obtain a state space representation for the plant $G(s)$ and the desired weighting function $W_1(s)$. From these, state space representations for $W_2(s)$, $G_0(s)$, and $G_1(s)$ must be calculated. These problems can be formulated as spectral factorization problems, and solved by methods similar to those discussed in Section 2.2.

4.3.1 Calculation of G_0

G_0 is a co-spectral factor of $M = G + G^\sim$, and thus can be calculated with the standard algorithm. The algorithm is restricted to systems G with a non-zero direct feedthrough term D. This is not a serious restriction, however. No finite-dimensional model is valid at all frequencies, nor does it need to be. This merely implies that rather than rolling off at high frequencies, $G(\infty)$ should be a constant.

First, define the state space representation of G as

$$G = \left[\begin{array}{c|c} A & B_2 \\ \hline C_2 & D_{22} \end{array}\right] = C_2 (sI - A)^{-1} B_2 + D_{22} \tag{4.42}$$

The reason for the selection of the subscripts on B, C, and D is that G is the (2,2) block of the four block problem.

G_0 can be represented as

$$G_0 = \left[\begin{array}{c|c} A & B_1 \\ \hline C_2 & D_{21} \end{array}\right] \tag{4.43}$$

where

$$D = D_{22} + D_{22}^T \tag{4.44}$$

$$A^{\times}_{M^T} = \begin{bmatrix} A^T & 0 \\ 0 & -A \end{bmatrix} - \begin{bmatrix} C_2 \\ -B_2^T \end{bmatrix} D^{-1} \begin{bmatrix} B_2 & C_2^T \end{bmatrix} \tag{4.45}$$

$$X_1 = Ric\left\{A^{\times}_{M^T}\right\} \tag{4.46}$$

$$B_1 = (B_2 + X_1 C_2^T) D^{-1/2} \tag{4.47}$$

$$D_{21} = D^{1/2} \tag{4.48}$$

From Chapter 2, Definition 5, the conditions required for this spectral factorization to be valid are:

(i) $M = M^{\sim}$,

(ii) M and M^{-1} are proper,

(iii) M and M^{-1} have no poles on the $j\omega$ axis, (or alternatively, M have no poles or zeroes on the $j\omega$ axis),

(iv) $M(\infty) > 0$.

The first condition is clearly satisfied, as is the second, since M and M^{-1} are proper with non-zero D_{22}. If G is a dereverberated mobility, then it has no imaginary poles, and thus neither does M. Furthermore, G is strictly positive real. This implies that $G(j\omega) + G^{\sim}(j\omega) > 0$, and thus that M has no zeroes on the $j\omega$ axis. This also implies that $M(\infty) > 0$.

4.3.2 Calculation of G_1

The (1,2) block of the four-block problem (4.34) is $G_1 G_0^{\sim}$. This has the stable poles, but the non-minimum phase zeroes of $M = G + G^{\sim}$. The state space algorithm for computing this is related to the spectral factorization algorithm found in [15], or Section 2.2, and only the differences between the two will be indicated here.

Given G as in Equation (4.42), then

$$M = G + G^{\sim} = \left[\begin{array}{cc|c} A & 0 & B_2 \\ 0 & -A^T & -C_2^T \\ \hline C_2 & B_2^T & D_{22} + D_{22}^T \end{array}\right] = \left[\begin{array}{c|c} A_M & B_M \\ \hline C_M & D \end{array}\right] \tag{4.49}$$

and

$$A_M^{\times} = \left[\begin{array}{cc} A & 0 \\ 0 & -A^T \end{array}\right] - \left[\begin{array}{c} B_2 \\ -C_2^T \end{array}\right] D^{-1} \left[\begin{array}{cc} C_2 & B_2^T \end{array}\right] \tag{4.50}$$

The spectral factorization algorithm in Section 2.2 relies on finding the modal spaces $\mathbf{X}_-(A_M^{\times})$ and $\mathbf{X}_+(A_M)$ corresponding to the left half-plane zeroes of M and the right half plane poles respectively. Instead, now find $\mathbf{X}_+(A_M^{\times})$ and $\mathbf{X}_+(A_M)$, corresponding to right half plane zeroes and right half plane poles. If these two spaces are complementary, then the required factorization exists.

Since the unstable poles of any matrix A are the stable poles of $-A$,

$$\mathbf{X}_+(A_M^{\times}) = \mathbf{X}_-(-A_M^{\times}) \tag{4.51}$$

Thus the desired factorization exists if $\mathbf{X}_-(-A_M^{\times})$ and $\mathbf{X}_+(A_M)$ are complementary. Since $A_M^{\times}$ is a Hamiltonian matrix, $-A_M^{\times}$ is as well. Thus, there exists a matrix

$$X_2 = Ric\left\{-A_M^{\times}\right\} \tag{4.52}$$

such that

$$\mathbf{X}_-(-A_M^{\times}) = \mathrm{Im}\left[\begin{array}{c} I \\ X_2 \end{array}\right] \tag{4.53}$$

and this is complementary to $\mathbf{X}_+(A_M)$, given by Equation (2.21). Given this, the remainder of the derivation follows Francis [15] or Section 2.2 exactly, so that

$$G_1(s)G_0(s) = \left[\begin{array}{c|c} A & B_2 \\ \hline D^{-1/2}(C_2 + B_2^T X_2) & D^{1/2} \end{array}\right] \tag{4.54}$$

$$= \left[\begin{array}{c|c} A & B_2 \\ \hline C_1 & D_{12} \end{array}\right] \tag{4.55}$$

Thus,

$$C_1 = D^{-1/2}(C_2 + B_2^T X_2) \tag{4.56}$$

$$D_{12} = D^{1/2} \tag{4.57}$$

Since the remaining (1,1) block $G_1 I$ of the four block problem is inner, it must be true that

$$D_{11} = 1 \tag{4.58}$$

Then the four block problem in Equation (4.34) is completely specified.

4.3.3 Calculation of W_2

The computation of the weighting function W_2 in Equation (4.37) from W_1 can also be represented in terms of a spectral factorization. First, represent W_1 in state space as

$$W_1 = \left[\begin{array}{c|c} A_w & B_w \\ \hline C_w & D_w \end{array}\right] \tag{4.59}$$

Then

$$W_1^{\sim} = \left[\begin{array}{c|c} -A_w^T & -C_w^T \\ \hline B_w^T & D_w^T \end{array}\right] \tag{4.60}$$

Combining these gives

$$W_1 W_1^{\sim} = \left[\begin{array}{cc|c} A_w & 0 & B_w \\ -C_w^T C_w & -A_w^T & -C_w^T D_w \\ \hline -D_w^T C_w & -B_w^T & -D_w^T D_w \end{array}\right] \tag{4.61}$$

The A matrix of this system is a Hamiltonian matrix, with the (1,2) block equal to zero. Thus the modal spaces are given by Equations (2.24) and (2.25). Hence define the similarity transformation

$$T = \left[\begin{array}{cc} I & 0 \\ X_w & I \end{array}\right] \tag{4.62}$$

where X_w satisfies the Lyapunov equation

$$A_w^T X_w + X_w A_w + C_w^T C_w = 0 \tag{4.63}$$

and use this to transform the system, Equation (4.61). This gives

$$W_1 W_1^{\sim} = \left[\begin{array}{cc|c} A_w & 0 & B_w \\ 0 & -A_w^T & -C_w'^T \\ \hline C_w' & -B_w^T & -D_w^T D_w \end{array}\right] \tag{4.64}$$

where

$$C_w' = B_w^T X_w + D_w^T C_w \tag{4.65}$$

Then W_2 is a spectral factor of

$$I - W_1 W_1^{\sim} = \left[\begin{array}{cc|c} A_w & 0 & B_w \\ 0 & -A_w^T & C_w'^T \\ \hline -C_w' & -B_w^T & I - D_w^T D_w \end{array}\right] \tag{4.66}$$

This is now in the form of a standard spectral factorization. In order to apply the algorithm, W_1 must satisfy

$$1 - D_w^T D_w > 0 \tag{4.67}$$

or $W_1(\infty) < 1$. This is not a limitation at all, since multiplying the weighting function everywhere by a constant will not change the resulting compensator. The other conditions specified in the definition of the spectral factorization are also satisfied. Note that if the magnitude of W_1 is less than one at all frequencies, then $1 - W_1 W_1^{\sim}$ can have no imaginary zeroes, nor can it have any imaginary poles.

4.3.4 Four Block Problem

Having determined how to compute all of its elements, the complete four-block problem can be written in state space form as

$$\left[\begin{array}{c|cc} A & B_1 & B_2 \\ \hline C_1 & D_{11} & D_{12} \\ C_2 & D_{21} & D_{22} \end{array}\right] \tag{4.68}$$

where

$$\mathcal{A} = \begin{bmatrix} A & 0 & 0 \\ B_w C_1 & A_w & 0 \\ 0 & 0 & A_w \end{bmatrix} \quad \mathcal{B}_1 = \begin{bmatrix} B_1 \\ B_w D_{11} \\ B_{w_2} \end{bmatrix} \quad \mathcal{B}_2 = \begin{bmatrix} B_2 \\ B_w D_{12} \\ 0 \end{bmatrix}$$

$$\mathcal{C}_1 = \begin{bmatrix} D_w C_1 & C_w & 0 \\ 0 & 0 & C_{w_2} \end{bmatrix} \quad \mathcal{D}_{11} = \begin{bmatrix} D_w D_{11} \\ D_{w_2} \end{bmatrix} \quad \mathcal{D}_{12} = \begin{bmatrix} D_w D_{12} \\ 0 \end{bmatrix} \tag{4.69}$$

$$\mathcal{C}_2 = \begin{bmatrix} C_2 & 0 & 0 \end{bmatrix} \qquad \mathcal{D}_{21} = \begin{bmatrix} D_{21} \end{bmatrix} \qquad \mathcal{D}_{22} = \begin{bmatrix} D_{22} \end{bmatrix}$$

The compensator is then found from the Riccati equations given in [16].

Chapter 5

Examples

5.1 Example 1: Free-Free Bernoulli-Euler Beam

As an example of the approach developed in the previous chapters, consider a free-free Bernoulli-Euler beam with a collocated force actuator and velocity sensor at one end, as shown in Figure 5.1. The dereverberated mobility for this system was calculated previously in Section 3.2. It is the transfer function of a semi-infinite beam, which can be found, for example, from the wave approach discussed in Section 2.3:

$$G(s) = \frac{\sqrt{2}}{(\rho A)^{3/4}(EI)^{1/4}} \cdot \frac{1}{\sqrt{s}} \tag{5.1}$$

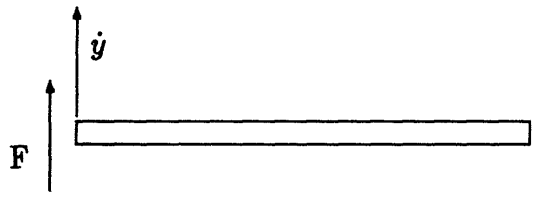

Figure 5.1: Bernoulli-Euler Free-Free Beam

For simplicity, assume the mass per unit length ρA and the bending stiffness EI are such that

$$G(s) = \frac{1}{\sqrt{s}} \tag{5.2}$$

This can be done without loss of generality, as it requires only a scaling of the plant.

First, consider the unconstrained optimal compensator that extracts the maximum possible energy. From Equation (4.17),

$$K(s) = \sqrt{-s} \tag{5.3}$$

This compensator has a slope of 10 db/decade, and a phase of $-45°$ at all frequencies. Note that this is the same compensator as that obtained by the unconstrained optimization in Miller *et al.* [28], though the derivation differs, and in Flotow and Schäfer [40], by setting the reflection coefficient corresponding to the creation of outgoing travelling waves from incoming travelling waves to zero. As expected, the unconstrained optimal compensator is noncausal and cannot be implemented. That it is noncausal could be determined by finding a rational approximation to $\sqrt{-s}$, which would have right half plane poles, or from the knowledge that $\sqrt{s}$ is stable and causal, since it is the transfer function of a stable structure (see Example 2 in the next section.) Since $\sqrt{s}$ is right half plane analytic, $\sqrt{-s}$ must be left half plane analytic, and therefore if it is stable, it must be noncausal.

Now, find the compensator that minimizes the maximum power flow into the structure. An analytical solution to this is given in Appendix A. With equal weighting at each frequency, ($W_1 = 1$) the optimal causal compensator is

$$K(s) = \sqrt{s} \tag{5.4}$$

This is similar to the noncausal solution, Equation (5.3), with the same magnitude everywhere, but a phase of $+45°$ instead. This is the "best" causal approximation to Equation (5.3), and dissipates exactly half of the incoming power at all frequencies.

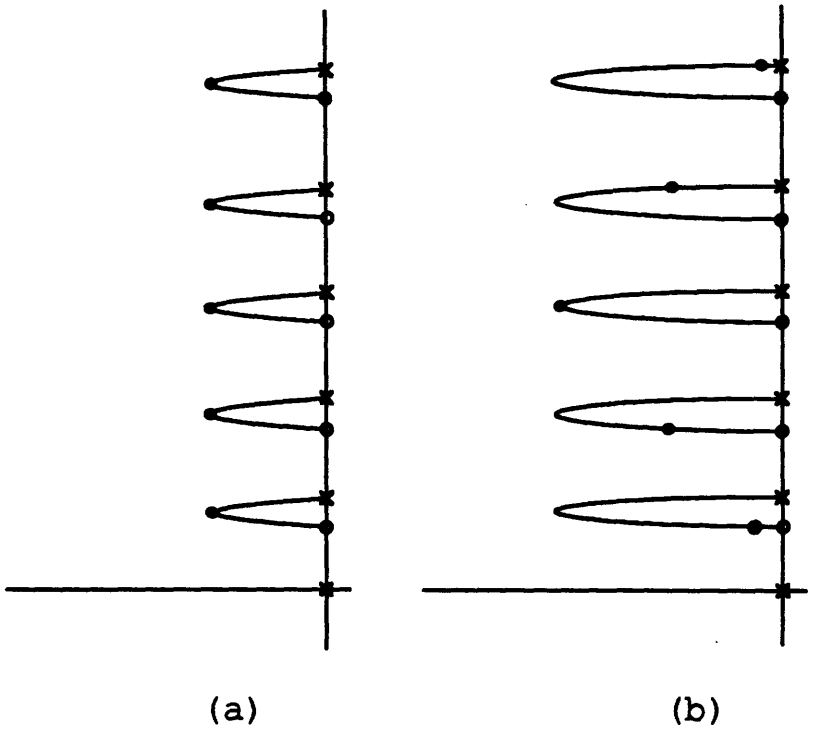

Figure 5.2: Schematic root locus with H_∞ design (a) and with velocity feedback (b).

Further insight into the nature of this control can be found from the root locus, shown schematically in Figure 5.2. With velocity feedback, an appropriate choice of gain will add significant damping to a given mode, and those nearby, but it is not possible to add significant damping to all of the modes at the same time. Thus the gain in velocity feedback must be optimized to provide damping at a certain frequency. Far enough away from this frequency, the gain is either too low to have much affect, or too high so that the closed loop poles lie near the open loop zeroes, which are undamped. With the optimal causal compensator $\sqrt{s}$, the locus is not as far into the left half plane, but now every pole can be placed at the leftmost part of its locus simultaneously. Ideally, one would like the root locus to be arbitrarily far into the left half plane, and place each pole at the leftmost part of its locus. This is the behavior obtained by the unconstrained optimal compensator $\sqrt{-s}$, which of

course cannot be implemented.

Now consider including a weighting function to increase the importance of a certain frequency range, say in a narrow band near 1 rad/sec. So select W_1 to have unit magnitude far from 1, and less than unit magnitude near 1 rad/sec. Recall that more importance is placed where the weighting function is smaller. An analytic solution here would be difficult. However, the plant in Equation (5.2) can be approximated adequately over a wide frequency range with a finite number of alternating poles and zeroes on the real axis, with equal logarithmic spacing. The state space methods described in Section 4.3 can then be used to obtain an approximate compensator. The resulting compensator is plotted in Figure 5.3, along with the optimal compensator with unity weighting from Equation (5.4), and the unconstrained optimum from Equation (5.3). Note that the magnitudes of these last two compensators are the same. Equation (5.2) in this case was approximated by 9 poles and 9 zeroes with frequencies from 10^{-4} to 10^{4} rad/sec. The weighting function W_1 had zeroes at $\frac{1}{\sqrt{2}}$ and $\sqrt{2}$, and poles at $\frac{1}{2\sqrt{2}}$ and $2\sqrt{2}$. Far from the region that was selected as important, the compensator still has a $\sqrt{s}$ behavior, though with less magnitude than the unweighted optimum in Equation (5.4), resulting in poorer performance. Near 1 rad/sec, though, the slope of the compensator is now -10 db/decade, and the phase is closer to $-45°$. At 1 rad/sec, the compensator has exactly the same magnitude, and almost the same phase as the noncausal optimum, and thus it absorbs almost all of the incoming power possible. The net power flow absorbed by this compensator is plotted in Figure 5.4, expressed as a fraction of the disturbance input power. For comparison, the power absorbed by velocity feedback and the unweighted optimum are also plotted in the same figure. The comparison between the two $\mathcal{H}_\infty$ designs illustrates the trade-off in the choice of the weighting function. The power flow can be increased in one frequency region, but at the expense of decreasing the power dissipation at all other frequencies.

If this control law is now applied to a finite beam, the closed loop performance

can be examined. The transfer function between force and velocity at the far (uncontrolled) end of the beam can be calculated using the phase closure approach of [27], discussed in Section 2.3. The beam length was chosen so that the fifth mode of the beam was at the center frequency of the weighted region. The result is plotted in Figure 5.5, and the envelope of the transfer function for any length beam is also plotted. As expected, the modal peaks in the region where W_1 is smallest are more heavily damped. Note that because the compensator in Figure 5.3 is positive real, it will not destabilize the beam at any length. (Nor will it destabilize any positive real structure.) Furthermore, for any length beam, there will be some damping achieved everywhere, and greater damping in the region of interest, as indicated by the envelope of possible transfer functions.

From Equation (4.39), the closed loop power flow can be related to the weighting function W_1. If the damping in a mode could be related to the power absorbed at the frequency of that mode, then the achieved damping could be predicted from knowledge of W_1 and the achievable $\mathcal{H}_\infty$ norm γ. For a simple beam, an approximation to this is relatively straightforward; the procedure is presented in Appendix B. With a unity weighting function W_1, the result is

$$\zeta_i = -\frac{\log(\gamma)}{\ell c_0 \sqrt{\omega_i}} \tag{5.5}$$

This can be compared with actual eigenvalue calculations, and while the result is not exact, the approximation is reasonable. Thus in this case, not only can the closed loop power flow be predicted without actually designing the compensator, the closed loop damping can also be predicted, provided one can give a reasonable estimate of γ. This would be useful for determining how to modify the weighting function to produce the desired behaviour.

It is worth comparing the results of this approach with those for other control design techniques. Methods such as LQG are difficult to compare due to the lack of a suitable basis for comparison. An LQG compensator will certainly give a better $\mathcal{H}_2$ norm of the quantity minimized than the $\mathcal{H}_\infty$ design approach for the

nominal model. For a sufficiently large perturbation in the plant, however, the LQG design may destabilize the system, as it has poor robustness to parametric model error. Another design technique which is more suitable for comparison is collocated velocity feedback. Rate feedback is also positive real, and thus guaranteed to be stabilizing, but the performance is expected to be worse, being suboptimal. A comparison of the power dissipated by rate feedback and by two $\mathcal{H}_\infty$ designs has already been shown in Figure 5.4. For a given structure, velocity feedback dissipates power with a specific frequency distribution, with the gain as the only parameter to vary. The gain changes only the center frequency of the distribution, and not its shape. The $\mathcal{H}_\infty$ design, on the other hand, allows much more freedom in the characteristics of the power dissipation with frequency. Greater dissipation at a single frequency is possible than with rate feedback, and broader band power dissipation is also achievable. The envelope of possible closed loop transfer functions on the free-free beam is shown in Figure 5.6 for several different gains of rate feedback, and for the unweighted $\mathcal{H}_\infty$ compensator described earlier. Once again, this illustrates the same point. Velocity feedback is stabilizing, but in general, it is suboptimal.

5.2 Example 2: Pinned-Free Beam

As a slightly more complicated example, consider again a finite beam, but this time with one end pinned, with a moment actuator and collocated angular rate sensor at this end. Also include some finite rotational inertia J at this end, as indicated in Figure 5.7. The theoretical dereverberated transfer function for this beam can be found once again using the wave approach of Section 2.3. For this structure, the boundary conditions at the pinned end are given by the matrices

$$B_u = \begin{bmatrix} 1 & 0 \\ 0 & \frac{JEI}{\rho A}k^4 \end{bmatrix} \tag{5.6}$$

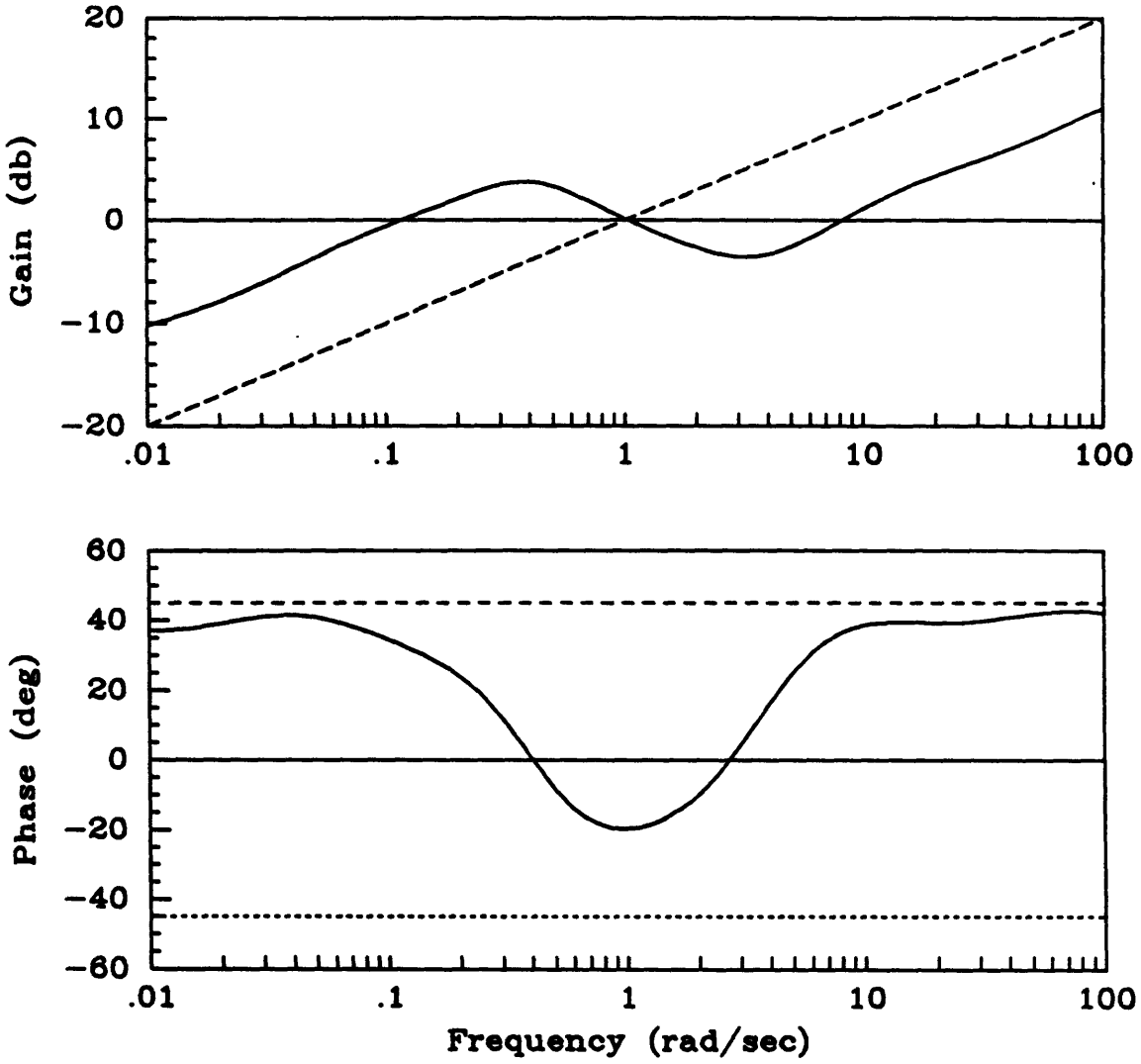

Figure 5.3: Optimal compensator for example 1 with weighting at 1 rad/sec (solid), with no weighting (dashed), and unconstrained (dotted).

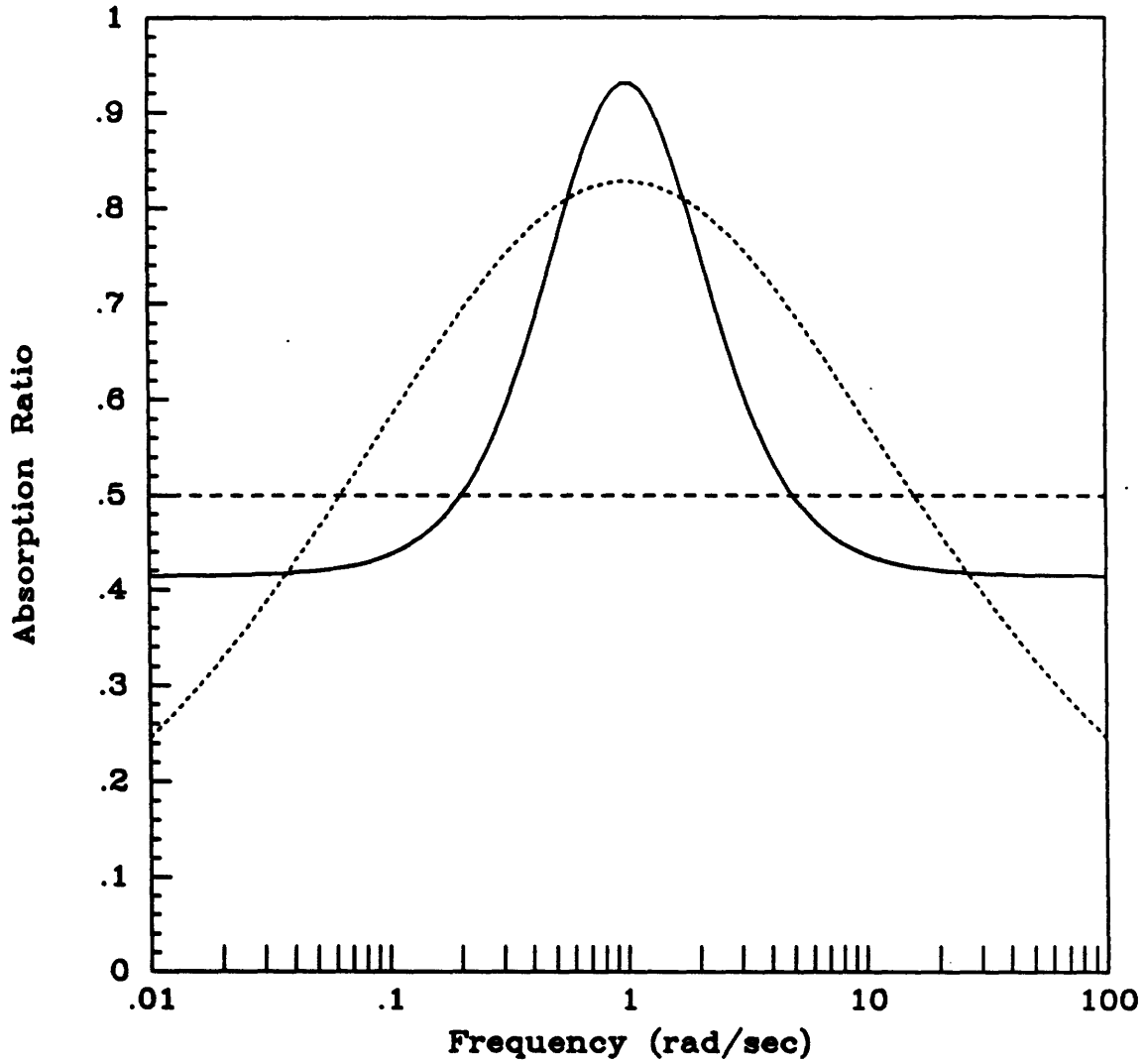

Figure 5.4: Power absorption for weighted $\mathcal{H}_\infty$ design (solid), velocity feedback (dotted), and unweighted $\mathcal{H}_\infty$ design (dashed).

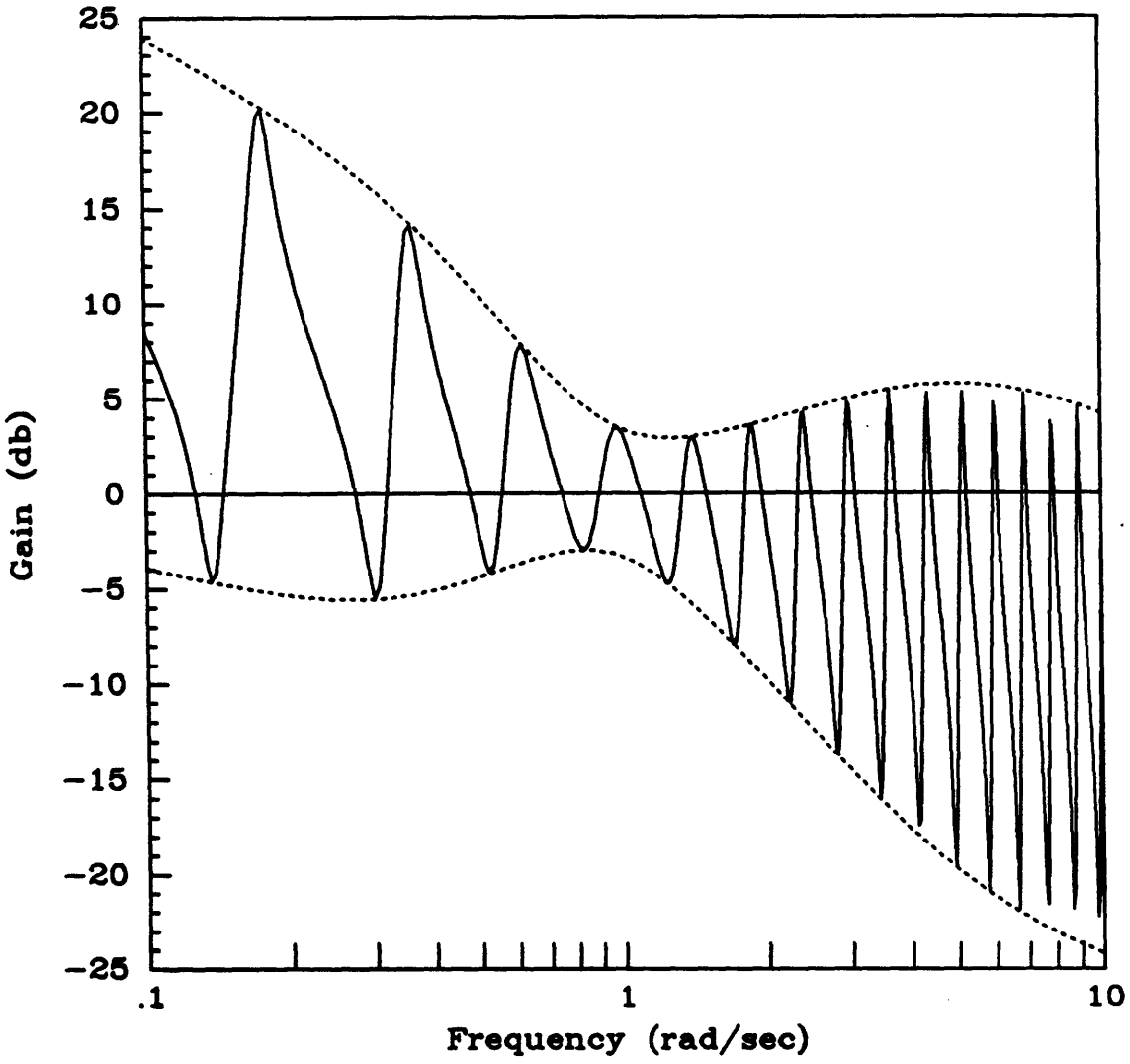

Figure 5.5: Closed loop transfer function at far end of beam (solid) and envelope of possible closed loop transfer functions (dotted).

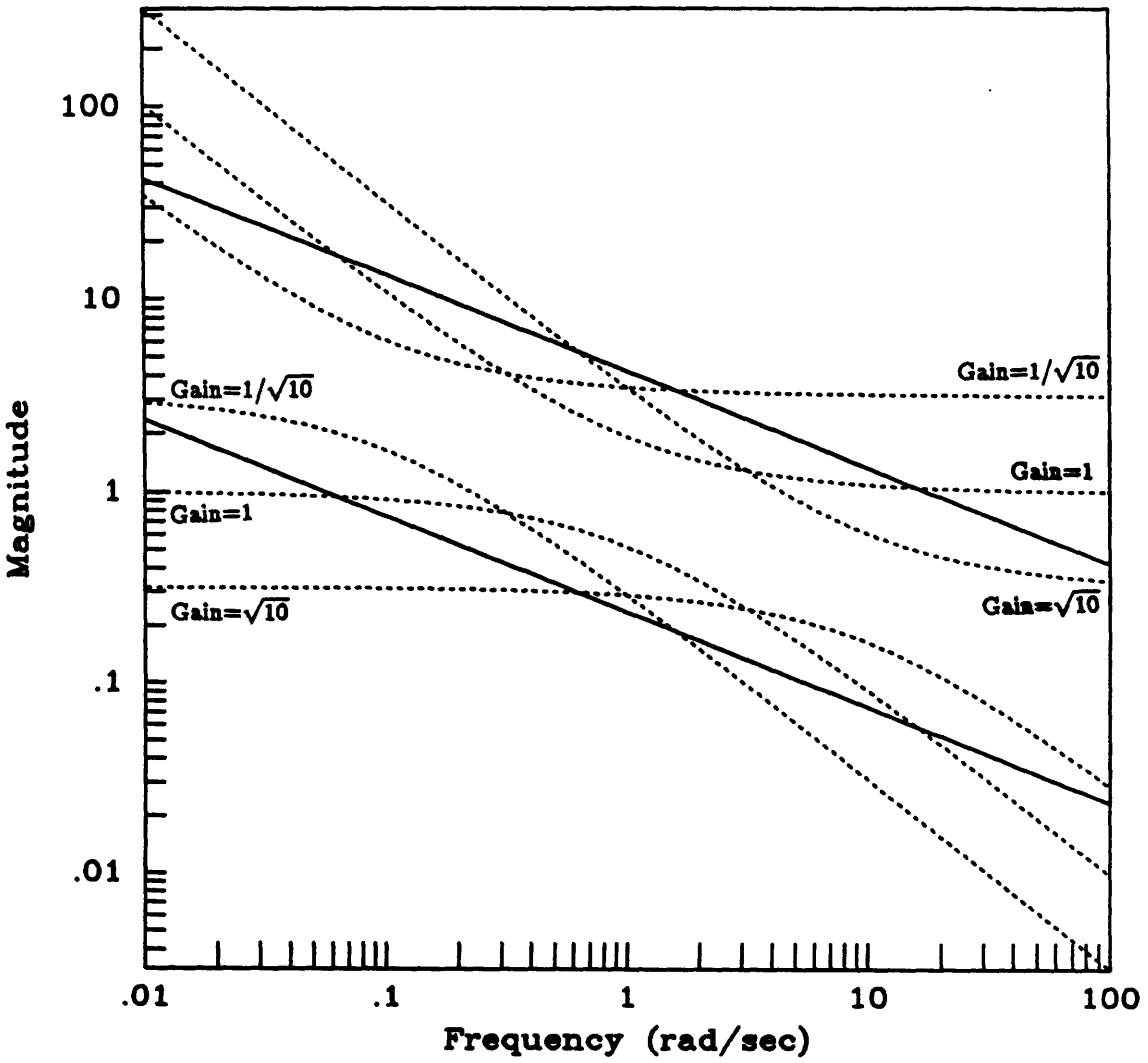

Figure 5.6: Envelope of possible closed loop transfer functions at far end of beam with different gains of rate feedback (dotted) and with unweighted $\mathcal{H}_\infty$ design (solid).

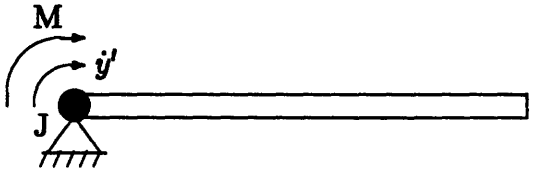

Figure 5.7: Bernoulli-Euler Pinned-Free Beam

$$B_f = \begin{bmatrix} 0 & 0 \\ 0 & 1 \end{bmatrix} \tag{5.7}$$

The wave number k is defined from Equation (2.52). So from Equations (2.40), (2.41), and (2.50),

$$\frac{\dot{y}'}{M} = \frac{s}{\sqrt{2}(\rho A)^{1/4}(EI)^{3/4}\sqrt{s} + Js^2} \tag{5.8}$$

If there were no rotational inertia J, then the transfer function would be

$$G(s) = \frac{\sqrt{s}}{\sqrt{2}(\rho A)^{1/4}(EI)^{3/4}} \tag{5.9}$$

The unconstrained optimal compensator would therefore be

$$K(s) = \frac{\sqrt{2}(\rho A)^{1/4}(EI)^{3/4}}{\sqrt{-s}} \tag{5.10}$$

This has a phase of 45°. If the weighting function W_1 was unity at all frequencies, then the causal optimum found from the $\mathcal{H}_\infty$ approach would be

$$K(s) = \frac{\sqrt{2}(\rho A)^{1/4}(EI)^{3/4}}{\sqrt{s}} \tag{5.11}$$

This has the same magnitude as the unconstrained optimum, but a phase of -45°. The calculations required to obtain these compensators are essentially the same as for the free-free beam in the previous example.

With $J \neq 0$, then at low frequencies, the behavior is similar to that of Equation (5.9). At high frequencies, the transfer function is dominated by the rotational

inertia, and rolls off at 20 db/decade. From the far end of the beam, the controlled end then behaves as if it were clamped, and regardless of the control, all disturbances are reflected back. Thus, power flow beyond the rolloff frequency of Equation (5.8) should be unimportant, and the weighting function here should be much larger than elsewhere. Also, assume again that some specific frequency range near 1 rad/sec is more important. Note that while in practice it would be difficult to extract power at high frequencies, the theory still allows power to be dissipated, due the presence of G_0. At high frequencies, $G \sim \frac{1}{Js}$, and hence $G_0 \rightarrow \infty$. Thus the disturbance spectrum is increased indefinitely to allow the same amount of power dissipation at all frequencies with the unconstrained compensator.

For computation, $EI = \frac{1}{\sqrt{2}}$ and $\rho A = \frac{1}{\sqrt{2}}$, so that the low frequency behavior is exactly $\sqrt{s}$. The rotational inertia J was selected to be 10^{-3}, to place the rolloff frequency at 100 rad/sec, at a slightly higher frequency than that considered to be important. Again, the system was approximated with a rational transfer function which is accurate over the frequency range of interest, from 10^{-4} to 10^{4} rad/sec.

The compensator for this case is shown in Figure 5.8. At low frequencies, the compensator is similar to the $\frac{1}{\sqrt{s}}$ that would be optimal with no rotary inertia and no weighting. Where the weighting function decreases near 1 rad/sec, the phase jumps towards the noncausal optimum phase of 45°, and thus absorbs close to the maximum power possible. At high frequencies, as desired, the compensator gives up and does not attempt to absorb incoming power, though it does remain positive real. Thus again, the closed loop system is stable for any length beam, and for any boundary condition at the far end. The open and closed loop transfer function from moment to slope rate at the controlled end of the beam is given in Figure 5.9. This transfer function shows the rolloff at 100 rad/sec, beyond which the poles and zeroes are essentially undamped, but almost cancel each other. The poles are more heavily damped near 1 rad/sec, but none of the zeroes are affected. Also plotted is the dereverberated mobility (Equation (5.8)), and the upper bound of the envelope

of possible transfer functions for any length of beam.

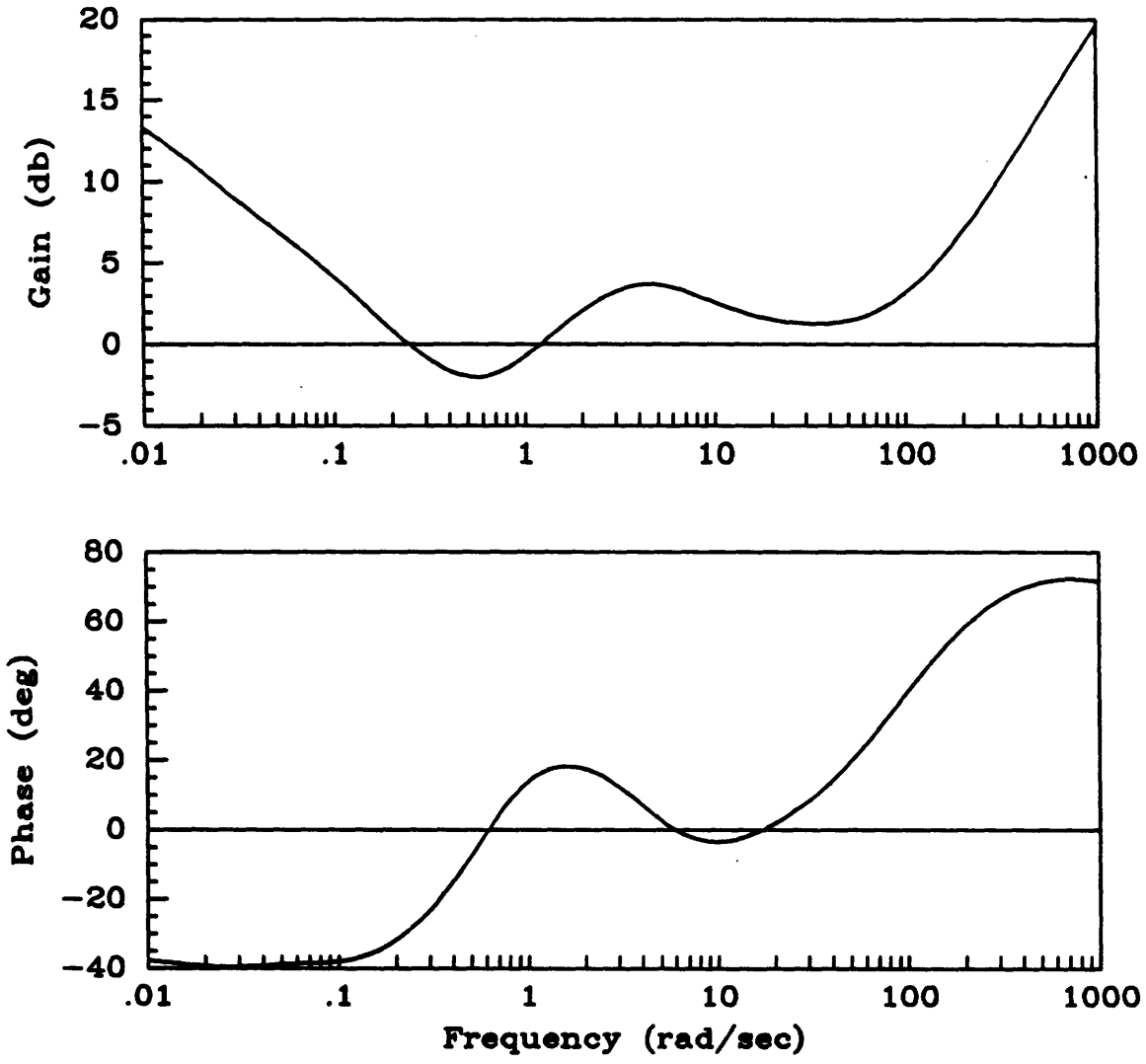

Figure 5.8: Optimal compensator for Example 2; pinned-free beam

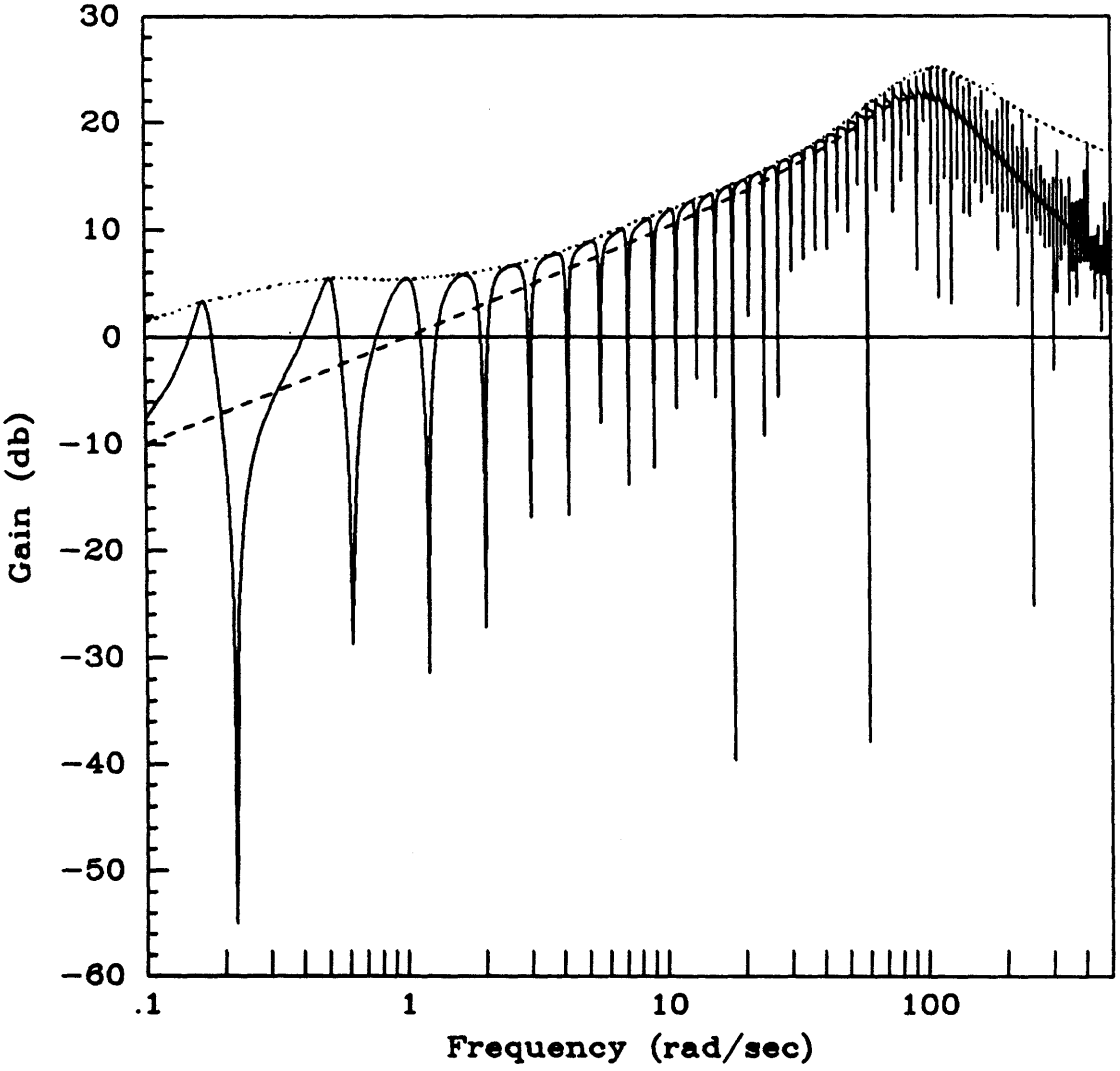

Figure 5.9: Closed loop transfer function at controlled end of pinned-free beam (solid), dereverberated mobility (dashed), and envelope of possible transfer functions (dotted).

Chapter 6

Experimental Results

While theoretical results are valuable of themselves, they must ultimately be tested in an experiment. This verifies the theoretical results, and indicates problems in their application. In addition to demonstrating the usefulness of the work, the experiment points out limitations, and appropriate directions for further research.

The approach described in Chapters 3 and 4 was tested on a brass beam suspended in the Space Engineering Research Center laboratory at M.I.T. Previous experiments with this beam [26,29] include collocated rate feedback and $\mathcal{H}_2$ optimal wave control, and these provide a basis for comparison with the $\mathcal{H}_\infty$ compensator.

6.1 Experimental Setup

The setup is shown schematically in Figure 6.1. For complete details on the setup, see reference [29]. The beam is suspended horizontally in the lab, with actuation and sensing such that the bending vibration can be controlled. One end is effectively pinned, while the other is free. The properties and dimensions of the beam are summarized in Table 6.1. The open-loop damping of the first 17 modes (up to a frequency of 27.7 Hz) averaged about 0.3%.

Control is applied through a torque motor at the pinned end, and sensing is

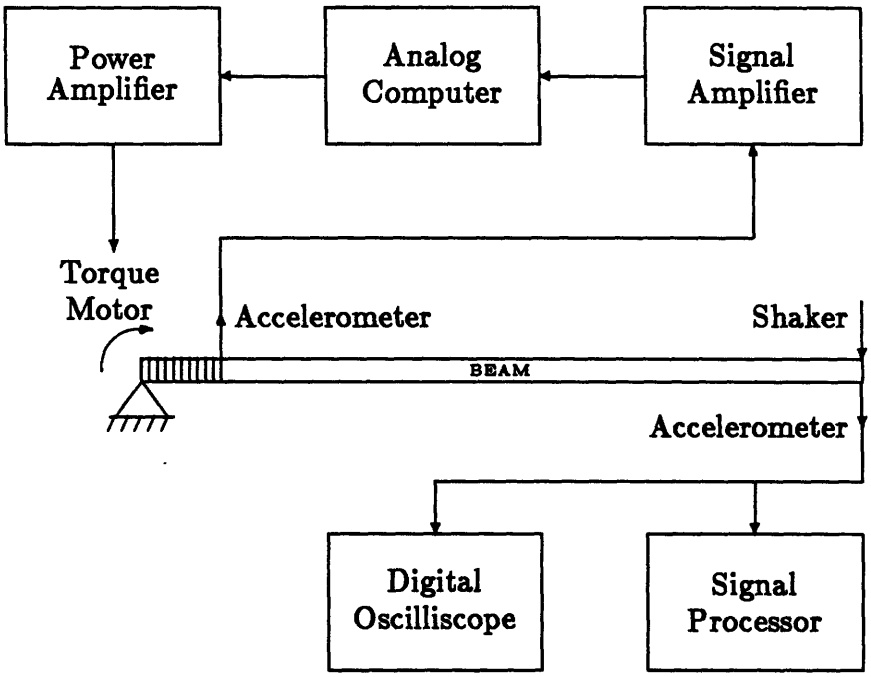

Figure 6.1: Schematic of Experimental Setup

Length	7.32 m
Width	0.102 m
Thickness	3.175 mm
EI	31.1 Nm^2
ρA	2.85 kg/m

Table 6.1: Beam Dimensions and Properties

provided by a linear accelerometer mounted a short distance from the end. The member connecting the sensor to the tip is assumed to be rigid, such that the sensor provides a rotational acceleration measurement collocated with the moment actuator. In practice, this assumption is not quite valid, though it is reasonable in the frequency range of interest.

In addition to the control actuator and sensor, a shaker and data acquisition accelerometer were mounted at the free end of the beam. The shaker was mounted to provide a force collocated with the acceleration measurement. The closed loop transfer function between these two was used as an indication of the performance achieved.

The signal from the accelerometer at the controlled end was fed through a signal amplifier into an analog computer which contained the compensator program. The output of this was fed through a power amplifier into the moment actuator. The accelerometer signal from the uncontrolled end was fed into a Signology SP-20 Signal Processing Peripheral to record and analyze the response data, and obtain frequency domain information. This signal was also fed into an oscilliscope so that any instabilities could be quickly identified, and their frequencies determined.

6.2 Compensator Design

A detailed model of the beam is not necessary for the experiment; it is sufficient to just take the transfer function from the control actuator to the control sensor. This transfer function is shown in Figure 6.2. The dereverberated mobility is that of Example 2, given in Equation (5.8) with the rotational inertia at the tip corresponding to the inertia of that part of the actuator armature and sensor that is fixed to the beam. From the measured transfer function, the effect of this inertia was at a frequency higher than the region of interest, so for the control design, the tip rotational inertia was assumed to be zero. The dereverberated mobility based

on this assumption is also shown in Figure 6.2.

The optimal compensator with unity weighting is proportional to $\frac{1}{\sqrt{s}}$, given in Equation (5.11). This compensator can also be derived from previous wave approaches, and had been implemented on this beam in [29]. In order to test the $\mathcal{H}_\infty$ approach, a weighting function was selected to emphasize a narrow frequency band near 35 rad/sec. This corresponds approximately to the frequency of the 7^{th} mode of the beam. The minimum value of W_1 in this region was approximately 0.65, and the weighting increased to near unity a factor of $\sqrt{2}$ above and below this frequency, as shown in Figure 6.3. The optimal compensator from slope rate to moment for this case was found to be well approximated by the product of the unweighted optimum, $\frac{1}{\sqrt{s}}$, and a two pole, two zero lag-lead network. This network provided the phase lead that is required so that at the center of the weighted region, the phase approaches the unconstrained optimal phase of 45° (from Equation (5.10)), allowing the compensator to dissipate more power. The optimum poles and zeroes of this network are symmetric about the center frequency of the weighting function W_1, at 35 rad/sec. The two free parameters of this network were optimized to minimize the $\mathcal{H}_\infty$ norm of the cost. This results in the compensator from slope rate to moment being

$$K(s) = 63.4 \cdot \frac{1}{\sqrt{s}} \cdot \left(\frac{s^2 + 38.5s + 466}{s^2 + 100s + 3210} \right) \tag{6.1}$$

The available measurement, however, was proportional to angular acceleration, and thus a further integration was necessary to obtain angular rate. This integrator was rolled off at DC to prevent saturation and drift problems. The second order dynamics were chosen to have a natural frequency of 0.5 Hz, and a damping ratio of 0.5. Finally, an additional gain was necessary to obtain the compensator from the sensor signal to the actuator input. The resulting compensator as implemented was

$$K(s) = 8110 \cdot \frac{1}{\sqrt{s}} \cdot \left(\frac{s^2 + 38.5s + 466}{s^2 + 100s + 3210} \right) \cdot \left(\frac{s}{s^2 + 3.14s + 9.87} \right) \tag{6.2}$$

The implementation of the half integrator $\frac{1}{\sqrt{s}}$ is presented in [26]. The transfer function of the circuit used to approximate this is shown in Figure 6.4. The approximation is excellent in the region of interest, however at higher frequencies, it rolls off too quickly, and there is an associated phase drop, as shown in Figure 6.4. The measured compensator in the experiment is compared with the desired compensator in Figure 6.5. Good agreement is obtained, except at low frequencies where the DC rolloff of the integrator has a noticeable effect, and at frequencies higher than those shown, where the approximation to $\frac{1}{\sqrt{s}}$ is poor. The actual compensator has some additional phase lead at 35 rad/sec, primarily due to the integrator dynamics, which results in increased damping at this frequency at the expense of poorer performance at low frequencies.

6.3 Results

Once the compensator was implemented, the gain was gradually turned from zero towards the optimal value. Because the actuator and sensor were not truly collocated, and had some dynamics, the plant was not actually positive real. Due to this, and because of the additional phase lag of the half integrator at high frequencies, the compensator could not be implemented at full gain without destabilizing high frequency modes of the beam. At 65% of the full gain, there was an instability at 775 Hz. (If a Bernoulli-Euler pinned free beam model were appropriate at this frequency, this would correspond to approximately the 90^{th} mode of the beam.) At 60% of the optimal gain, a significant improvement in the response of the beam was already apparent, as shown in Figure 6.6. This figure compares the open loop with the closed loop transfer function from force at the free end to collocated velocity. The corresponding open and closed loop transfer functions for velocity feedback can be found in [29]. The results for the $\mathcal{H}_\infty$ technique presented here show some improvement over rate feedback already, even though full gain was not used. As

desired, the modes in one particular frequency range are damped more heavily than others. This range is slightly higher in frequency than that desired due to the implementation at less than the optimal gain. Note that the spikes present in the data at 16.4, 19.8, 24.3, and 24.5 Hz correspond to torsional modes of the beam, which are excited by the shaker but are uncontrolled by the moment actuator.

The predicted response based on the implemented compensator is plotted in Figure 6.7. This was calculated from the experimental compensator transfer function using the approach of Section 2.3. Reasonable agreement is obtained between this prediction and the actual transfer function, although the achieved performance is noticeably better than that predicted. A prediction based on the desired, optimal compensator would be poorer due to the significant additional phase lead at 35 rad/sec in the actual compensator.

Further experimentation is still necessary. The implementation of the compensator could be improved at both low and high frequencies, and this might allow better performance to be achieved, at a higher gain. Ideally, the experiment should be done on a structure with truly collocated sensors and actuators. This could be done on this beam by mounting a tachometer on the torque motor. Ultimately, however, in any experiment, the input to output transfer function will not remain positive real for sufficiently high frequencies, and the compensator design should be modified to recognize this fact. This could be done after the $\mathcal{H}_\infty$ approach developed in this thesis has been applied, by including additional roll-off in an *ad hoc* manner. This would reduce the complementary sensitivity at higher frequencies, so that the singular value test of Slater [37] could be passed. Alternatively, and preferentially, the singular value constraint could be embedded in the design process. Thus this experiment has indicated at least one direction that future research into this control design approach should take.

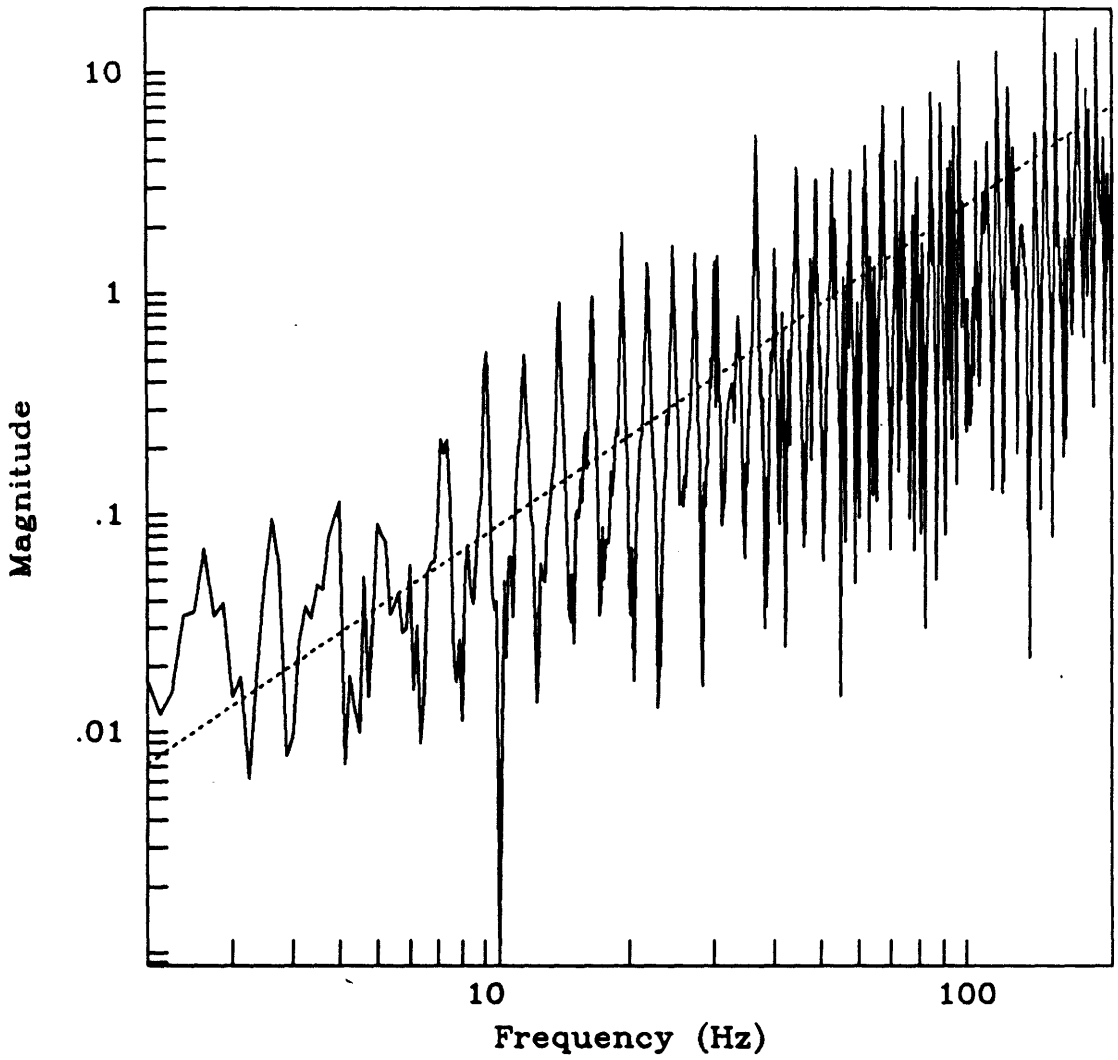

Figure 6.2: Open loop transfer function at controlled end of beam (solid), and dereverberated mobility used for control design (dotted).

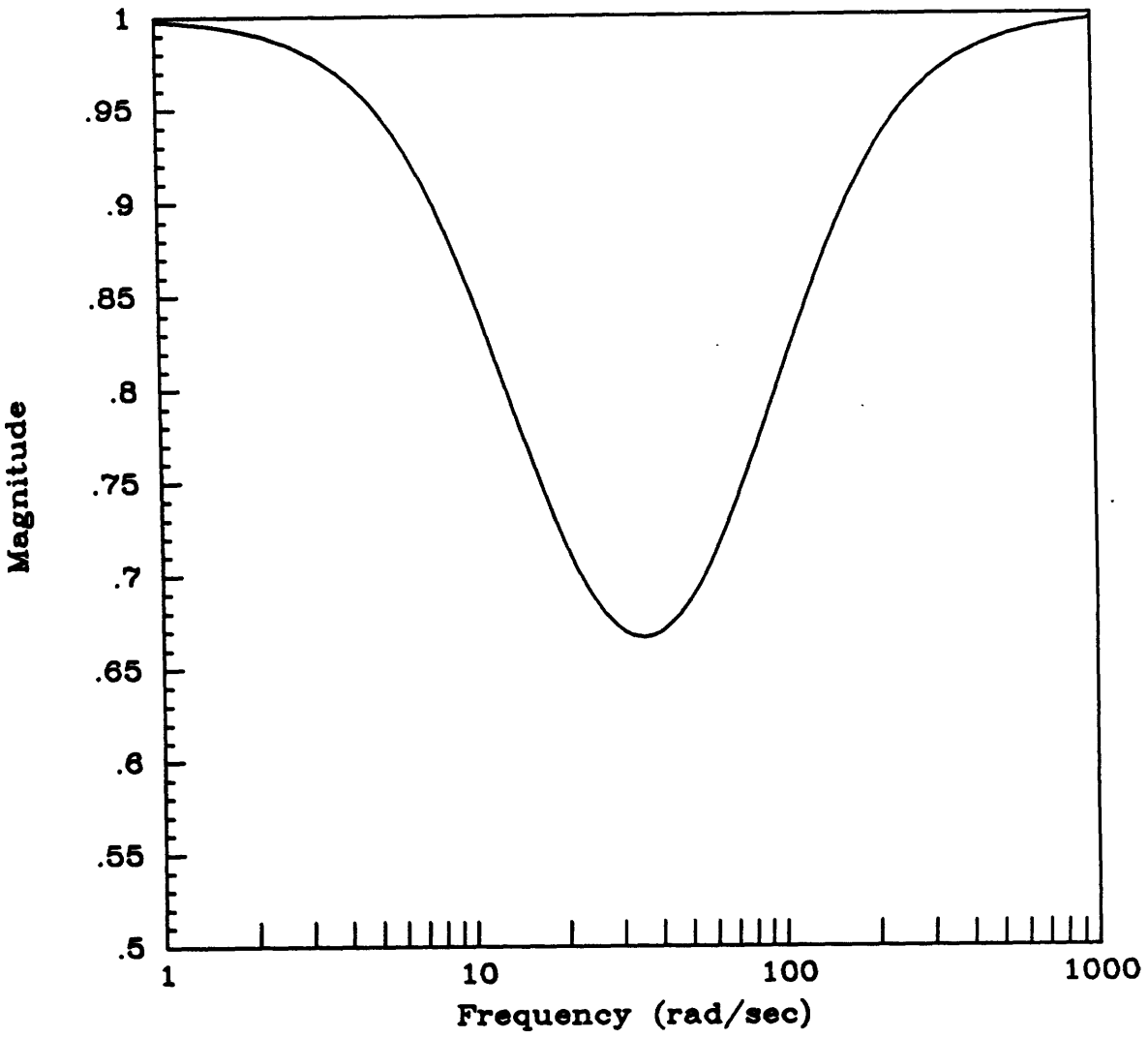

Figure 6.3: Weighting function W_1 used for control design in experiment.

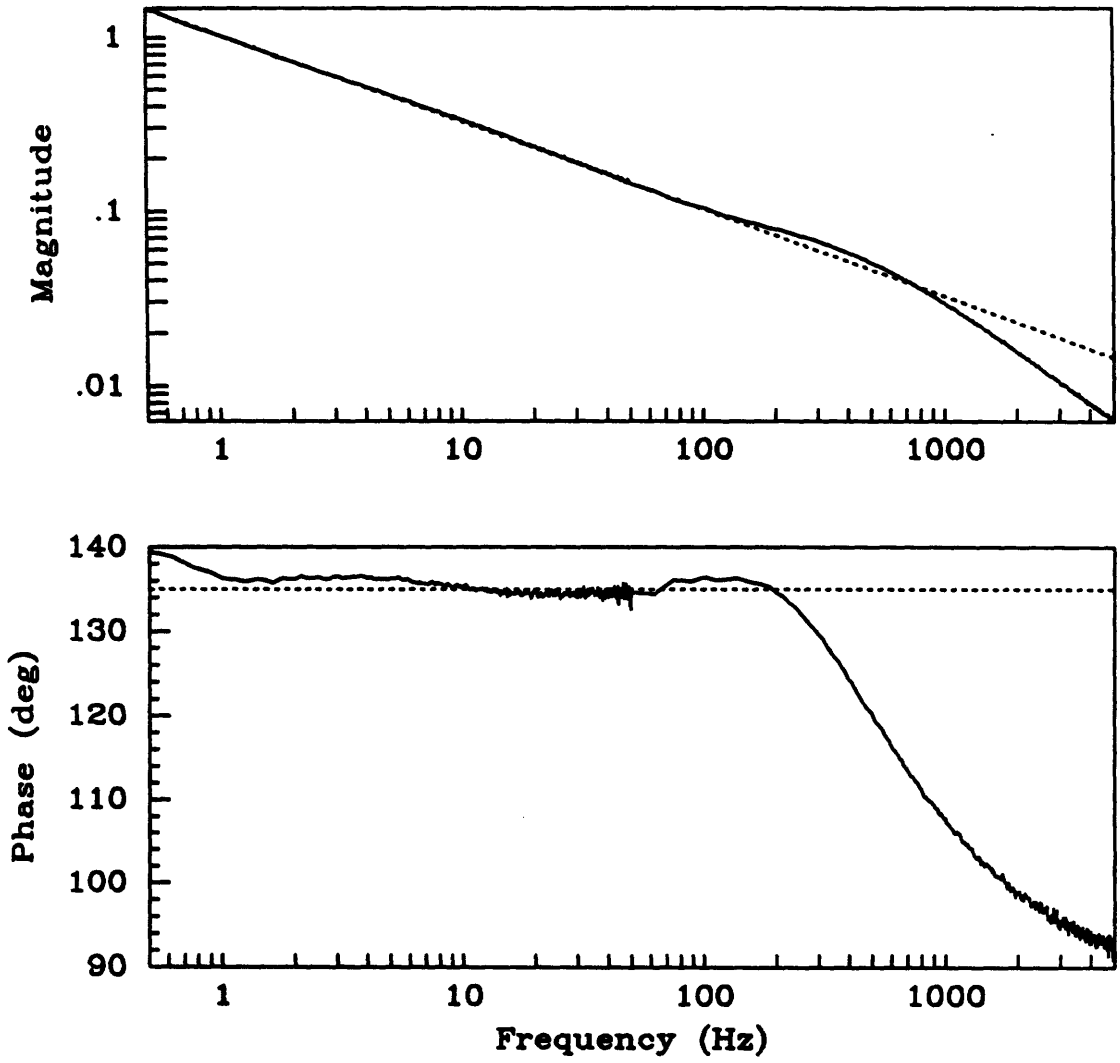

Figure 6.4: Transfer function of half integrator implemented in experiment (solid), and ideal half integrator (dotted).

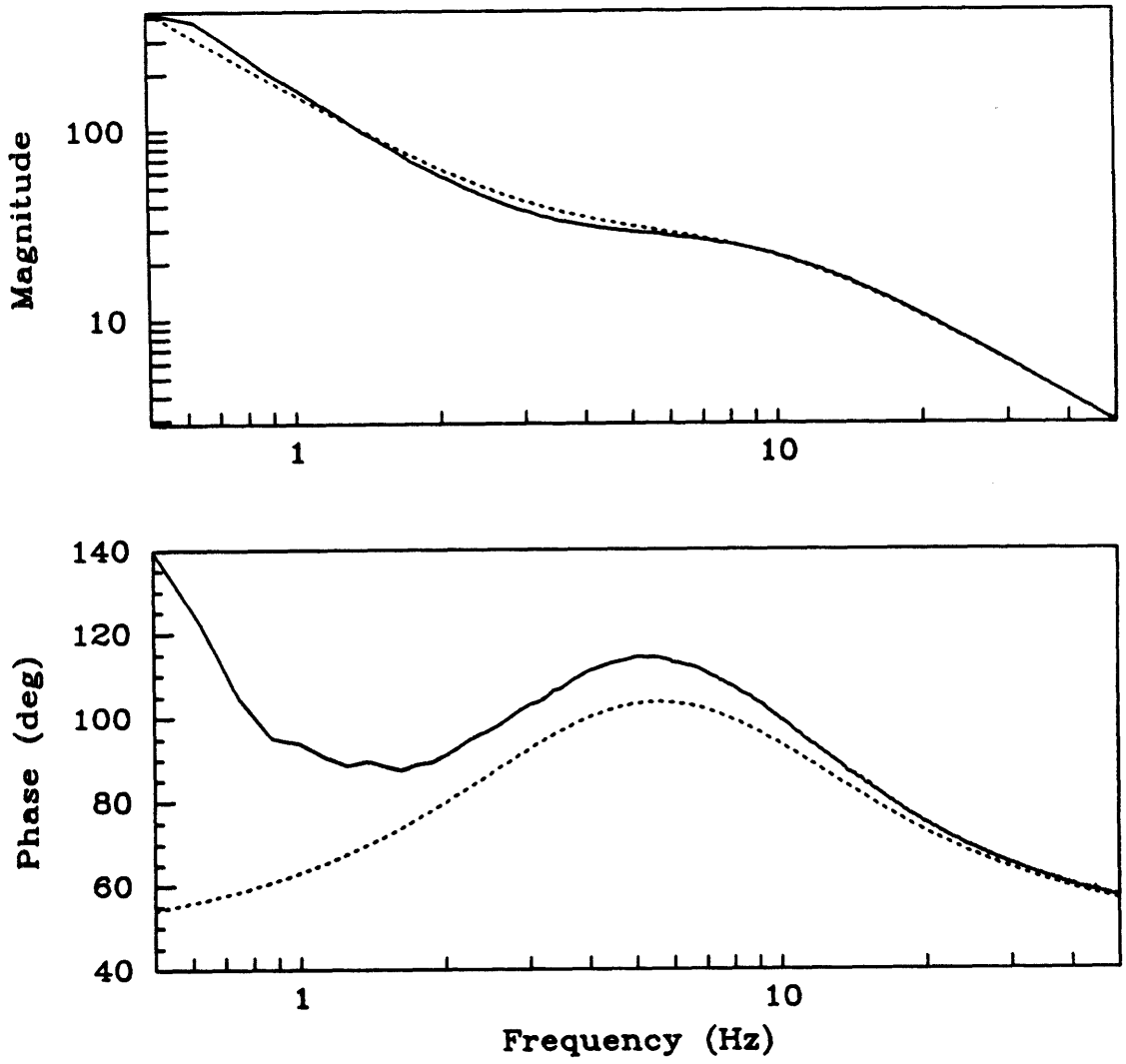

Figure 6.5: Transfer function of compensator implemented in experiment (solid), and desired compensator (dotted).

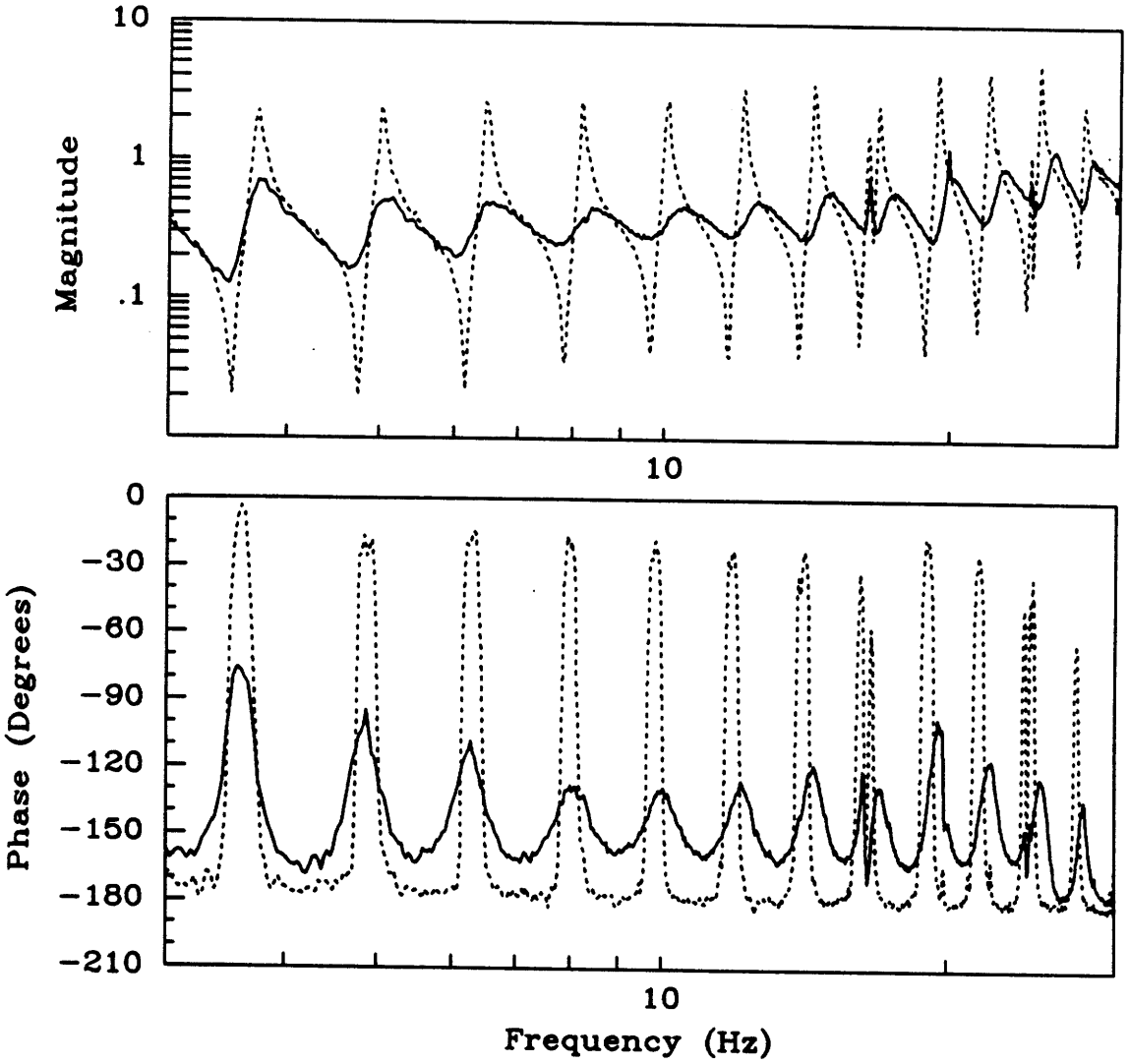

Figure 6.6: Experimental open (dotted) and closed loop (solid) transfer functions.

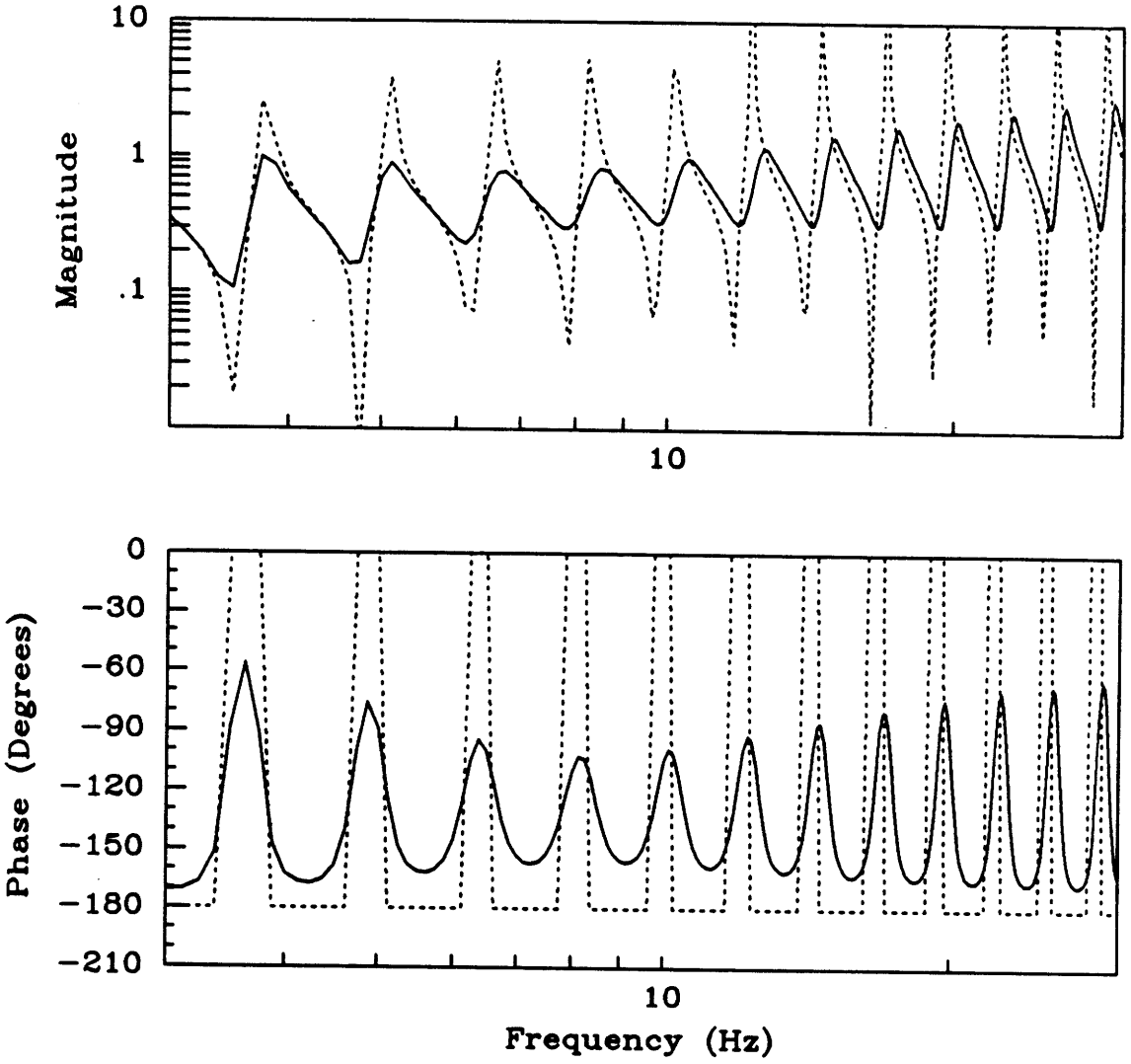

Figure 6.7: Predicted open (dotted) and closed loop (solid) transfer functions.

Chapter 7

Conclusions and Recommendations

7.1 Summary

In this thesis an approach to broadband active damping of modally dense structures with significant uncertainty has been presented. Both modelling and control design issues for this class of problems were investigated. Instead of a wave-based or modal model, the structure is modelled with its dereverberated mobility. The maximum power flow into the structure is minimized by solving an equivalent $\mathcal{H}_\infty$ control problem.

7.2 Contributions and Conclusions

1. A wave based model of the local dynamics of a structure near a collocated and dual sensor and actuator pair is equivalent to a dereverberated model of the structure. The dereverberated model is more general than a local wave model, as it can be easily applied to any structure. This model can be calculated directly from the driving point impedance, by

taking its logarithmic average, and can therefore be applied even when only experimental data are available. The dereverberated model retains many of the advantages of wave models. The local information can be determined with less uncertainty than the full structural model, while the global dynamics of the structure can be modified by controlling the local dynamics near an actuator, with a control law based only on this local model.

2. A causal, guaranteed stabilizing, optimal compensator can be obtained by minimizing the maximum power flow into the structure. This results in a positive real controller which dissipates power at all frequencies. This can be compared with several other compensators that could be designed based on the same model. The compensator that dissipates the most power at every frequency is in general noncausal, and cannot be implemented. $\mathcal{H}_2$ optimal power dissipation [28] does not guarantee stability, and simple rate feedback is stabilizing, but not necessarily optimal. The desirable properties of the solution can be retained while increasing the importance of a certain frequency range, through the use of a weighting function.

3. The technique was demonstrated for several simple examples. If a weighting function is chosen to emphasize some frequency range, then at the frequency deemed most important, the optimal compensator is close in both magnitude and phase to the unconstrained optimum. Thus at this frequency, it dissipates almost all of the incoming power possible. The compensator still dissipates some power at all frequencies, and is therefore guaranteed to be stable. The unconstrained optimal compensator thus provides some insight into how one could select the best compensator without requiring the $\mathcal{H}_\infty$ design approach. The transfer function should be chosen to match the unconstrained transfer function as closely

as possible in both magnitude and phase at the frequencies deemed important, while maintaining causality and positive realness.

4. Experimental results indicate that this approach to modelling and control design performs satisfactorily. Significant damping was added to many modes of a laboratory structure, without the large effort in system identification, off-line computation, and compensator complexity that would be required of many control design techniques. Greater damping was achieved than in velocity feedback experiments on the same structure [29]. Difficulties arose, however, for two main reasons. First, the implementation of the compensator was not perfect, particularly at low and high frequencies. Second, and more important, the actuator and sensor were not collocated, and may have had additional dynamics, so that the plant transfer function was not positive real at all frequencies as assumed.

7.3 Recommendations

1. The approach presented in this thesis works for systems which have a positive real transfer function between the sensor and actuator. In real structures, this will never be the case, due to actuator and sensor dynamics, time delays, and noncollocated actuators and sensors. Further work should investigate ways to modify the control design technique to allow for perturbations from the positive real condition, for example using the results of Slater [37]. One approach to doing this was discussed briefly in Chapter 4. Stability can be guaranteed by solving an $\mathcal{H}_\infty$ minimization problem, with a constraint on the $\mathcal{H}_\infty$ norm of a second transfer function. Whether this problem can be easily solved is an open question.

2. Further experimentation is necessary to obtain a better comparison between this technique and existing control design approaches. On the struc-

ture used in the experiment in Chapter 6, this could include a better implementation of the compensator, and either a hardware modification to give a collocated sensor and actuator, or some allowance in the compensator design procedure for non-collocation. Also, the experiment was conducted on a structure which could be easily modelled with a wave approach. Experimental results on a more complex structure for which this is not the case would be valuable in justifying the modelling approach presented in this thesis.

3. There may be a relationship between the modelling and control design approach presented here, and existing approaches, such as MEOP [5] and other optimal wave control methods [28]. These connections should be investigated. In particular, Miller *et al.* [28] solved an $\mathcal{H}_2$ optimal control problem, while this research solved a similar $\mathcal{H}_\infty$ problem. A combination of these two problems would be of interest. Closed loop stability can be guaranteed with an $\mathcal{H}_\infty$ constraint, and an $\mathcal{H}_2$ optimization could then guarantee performance [6,31]. Depending on the value of the constraint, this approach could yield solutions varying from the $\mathcal{H}_\infty$ optimal solution presented here, to the $\mathcal{H}_2$ optimal solution of Miller *et al.* [28].

4. The approach presented in this thesis optimizes the power dissipation associated with the control input, which results in active damping of the structure. However, damping is not necessarily a suitable performance criterion for all structural control problems. The algorithm should be modified to allow for the evaluation and optimization of other performance criteria, such as line-of-sight pointing error.

5. In general, the first few modes of a structure are relatively well known, and the uncertainty increases with frequency. A compensator which discards this information is suboptimal. An additional modification to the

approach should be to incorporate some knowledge of the lowest modes of the structure.

References

[1] Anderson, B.D.O., "A System Theory Criterion For Positive Real Matrices," *SIAM Journal of Control,* Vol. 5, No. 2, 1967, pp. 171-182.

[2] Aubrun, J-N., "Theory of the Control of Structures by Low-Authority Controllers," *AIAA Journal of Guidance and Control,* Vol. 3, No. 5, Sept-Oct 1980, pp. 444-451.

[3] Balas, M.J., "Feedback Control of Flexible Systems," *IEEE Transactions on Automatic Control,* Vol. AC-23, No. 4, Aug. 1978.

[4] Balas, M.J., "Trends in Large Space Structure Control Theory: Fondest Hopes, Wildest Dreams," *IEEE Transactions on Automatic Control,* Vol. AC-27, No. 3, June 1982, pp. 522-535.

[5] Bernstein, D.S. and Hyland, D.C., "Optimal Projection for Uncertain Systems (OPUS): A Unified Theory of Reduced Order, Robust Control Design," in *Large Space Structures: Dynamics and Control,* Atluri and Amos (ed.), Springer-Verlag, 1988.

[6] Bernstein, D.S. and Haddad, W.M. "LQG Control with an $\mathcal{H}_\infty$ Performance Bound: A Riccati Equation Approach," *IEEE Transactions on Automatic Control,* Vol. 34, No 3, March 1989, pp. 293-305.

[7] Blackwood, G.H., Chu, C-C., Fanson, J.L., and Sirlin, S.W., "Uncertainty Modeling for the Control of an Active Structure," to be presented at the ASME 1989 Winter Meeting, San Francisco, CA, Dec. 1989.

[8] Bode, H.W., *Network Analysis and Feedback Amplifier Design,* Van Nostrand, New York, 1945.

[9] Boulahbal, D., *Investigations on Group Delay in Structures and Acoustical Spaces,* 1988 SM Thesis, Department of Mechanical Engineering, M.I.T., Cambridge, MA.

[10] Chen, G-S., Lurie, B.J., and Wada, B.K., "Experimental Studies of Adaptive Structures For Precision Performance," *Proceedings of the* 30^{th} *Structures, Structural Dynamics and Materials Conference,* Mobile, AL, April 1989, pp. 1462-1472.

[11] Doyle, J.C. and Stein, G., "Multivariable System Design: Concepts for a Classical/Modern Synthesis," *IEEE Transactions on Automatic Control,* Vol. AC-26, No. 1, Feb. 1981, pp. 4-16.

[12] Doyle, J.C., "Analysis of Feedback Systems with Structured Uncertainties," *IEE Proceedings,* Vol. 129, Part D, No. 6, Nov. 1982, pp. 242-250.

[13] Doyle, J.C., Glover, K., Khargonekar, P.P., and Francis, B.A., "State-Space Solutions to Standard $\mathcal{H}_2$ and $\mathcal{H}_\infty$ Control Problems," *IEEE Transactions on Automatic Control,* Vol. 34, No. 8, Aug. 1989, pp. 831-847.

[14] Ewins, D.J., *Modal Testing: Theory and Practice,* John Wiley & Sons, New York, NY, 1986, p. 27.

[15] Francis, B.A., *A Course in* $\mathcal{H}_\infty$ *Control Theory,* Springer-Verlag 1987.

[16] Glover, K., and Doyle, J.C., "State-Space formulae for all Stabilizing Controllers That Satisfy an $\mathcal{H}_\infty$-Norm Bound and Relations to Risk Sensitivity," *Systems and Control Letters,* 12 (1988) 167-172.

[17] Hagedorn, P., and Schmidt, J.T., "Active Vibration Damping of Flexible Structures Using the Travelling Wave Approach," *Proceedings of the Second International Symposium on Spacecraft Flight Dynamics,* Darmstadt, FR Germany, Oct. 1986, ESA SP-255, Dec. 1986.

[18] Hall, S.R., Crawley, E.F., How, J.P., and Ward, B., "A Hierarchic Control Architecture for Intelligent Structures," submitted to *AIAA Journal of Guidance Control and Dynamics,* (Space Systems Laboratory Report #19-88, M.I.T., Cambridge, MA.)

[19] Hodges, C.H. and Woodhouse, J., "Theories of Noise and Vibration Transmission in Complex Structures," *Reports on Progress in Physics,* 1986 **49** pp. 107-170.

[20] How, J.P., *An Analysis of Local Control Designs for a Hierarchic Control Architecture for Intelligent Structures,* 1989 SM Thesis, Department of Aeronautics and Astronautics, M.I.T., Cambridge, MA.

[21] Lyon, R.H., *Statistical Energy Analysis of Dynamical Systems: Theory and Applications,* The MIT Press, Cambridge MA, 1975.

[22] Lyon, R.H., *Machinery Noise and Diagnostics,* Butterworth Publishing, June 1987.

[23] Mace, B.R. "Active Control of Flexural Vibrations," *Journal of Sound and Vibration,* **114**, 253-270, 1987.

[24] MacMartin, D.G. and Hall, S.R., "An $\mathcal{H}_\infty$ Power Flow Approach to Control of Uncertain Structures," submitted to *AIAA Journal of Guidance Control and Dynamics,* (Space Systems Laboratory Report #10-89, M.I.T., Cambridge, MA.)

[25] Milich, D.A., *A Methodology for the Synthesis of Robust Feedback Systems,* 1988 PhD Thesis, Department of Mechanical Engineering, M.I.T., Cambridge, MA. (Laboratory for Information and Decision Systems Report LIDS-TH-1748.)

[26] Miller, D.W., *Modelling and Active Modification of Wave Scattering in Structural Networks,* 1988 ScD Thesis, Department of Aeronautics and Astronautics, (Space Systems Laboratory Report #12-88), M.I.T., Cambridge, MA.

[27] Miller, D.W., "Power Flow in Structural Networks," *Journal of Sound and Vibration,* **128**, 145-162, 1989.

[28] Miller, D.W., Hall, S.R. and von Flotow, A.H., "Optimal Control of Power Flow at Structural Junctions," *Proceedings of the 1989 American Control Conference,* Pittsburgh, PA, June 1989.

[29] Miller, D.W., and Hall, S.R., "Experimental Results Using Travelling Wave Power Flow Techniques," to be presented at the ASME 1989 Winter Meeting, San Francisco, CA, Dec. 1989.

[30] Mustafa, D., and Glover, K., "Controllers Which Satisfy a Closed-Loop $\mathcal{H}_\infty$-Norm Bound and Maximize an Entropy Integral," *Proceedings IEEE Conference on Decision and Control,* Austin TX, Dec. 1988.

[31] Mustafa, D., "Relations Between Maximum-Entropy/$\mathcal{H}_\infty$ Control and Combined $\mathcal{H}_\infty$/LQG Control," *Systems and Control Letters* 12 (1989) 193-203.

[32] Pines, D.J., and von Flotow, A.H., "Active Control of Bending Wave Propagation at Acoustic Frequencies," *Proceedings of the 1989 American Control Conference,* Pittsburgh, PA, June 1989.

[33] Redman-White, W., Nelson, P.A., and Curtis, A.R.D., "Experiments on the Active Control of Flexural Wave Power Flow," *Journal of Sound and Vibration,* **112**, 187-191, 1987.

[34] Rhee, I., and Speyer, J.L., "A Game Theoretic Controller and Its Relationship to H_∞ and Linear-Exponential-Gaussian Synthesis," to be presented at the 28^{th} IEEE Conference on Decision and Control, Tampa, Florida, Dec. 1989.

[35] Scheuren, J., "Active Control of Bending Waves in Beams," *Internoise,* Munich, 591-594, Sept. 1985.

[36] Skudrzyk, E. "The mean-value method of predicting the dynamic response of complex vibrators," *Journal of the Acoustical Society of America,* **67**(4), April 1980.

[37] Slater, G.L., Zhang, Q., and Bosse, A., "Robustness with Positive Real Controllers for Large Space Structures," *Proceedings of the 1989 AIAA Guidance, Navigation, and Control Conference,* Boston, MA, August 1989, pp. 932-941.

[38] Tribolet, J.M., and Quatieri, T.F., "Computation of the Complex Cepstrum," in *Programs for Digital Signal Processing,* IEEE Press Book, Ed. by IEEE, ASSP, New York, 1979.

[39] Vaughan, D.R., "Application of Distributed Parameter Concepts to Dynamic Analysis and Control of Bending Vibrations," *Journal of Basic Engineering,* June 1968, pp. 157-166.

[40] von Flotow, A.H., and Shäfer, B., "Wave-Absorbing Controllers for a Flexible Beam," *AIAA Journal of Guidance, Control, and Dynamics,* Vol. 9, No. 6, Nov.-Dec. 1986, pp. 673-680.

[41] von Flotow, A.H., "The Acoustic Limit of Structural Dynamics," in *Large Space Structures: Dynamics and Control,* Atluri and Amos (ed.), Springer-Verlag, 1988.

[42] Zhang, Z., and Freudenberg, J.S., "State-Space Formulas for Inner-Outer Factorization," *Proceedings of the 1989 American Control Conference,* Pittsburgh, PA, June 1989.

Appendix A

Beam $\mathcal{H}_\infty$ Compensator

For a free-free beam with dereverberated mobility $G(s) = \frac{1}{\sqrt{s}}$, the compensator that minimizes the maximum power flow into the structure can be found analytically. From Equation (4.30) the problem is to find a stable, causal compensator that minimizes the $\mathcal{H}_\infty$ norm of the transfer function from w to $G_0^{\sim}u + w$. From the definition of G_0 (Equation (4.23)),

$$G_0 G_0^{\sim} = \frac{1}{\sqrt{s}} + \frac{1}{\sqrt{-s}} \tag{A.1}$$

$$= \frac{\sqrt{2}}{\sqrt[4]{s}\sqrt[4]{-s}} \tag{A.2}$$

Or,

$$G_0(s) = \frac{\sqrt[4]{2}}{\sqrt[4]{s}} \tag{A.3}$$

Since $d = G_0 w$, then from Equation (4.4),

$$u = H G_0 w \tag{A.4}$$

The compensator K from y to u will be stable and causal provided H is also stable and causal. Thus the problem is to find H to minimize

$$\|G_0^{\sim} H G_0 + 1\|_\infty \tag{A.5}$$

The solution to this, using the notation of Francis [15] is

$$\gamma = \min_H \|G_0^{\sim} H G_0 + 1\|_\infty \tag{A.6}$$

$$= \min_H \left\| \frac{\sqrt[4]{2}}{\sqrt[4]{-s}} H \frac{\sqrt[4]{2}}{\sqrt[4]{s}} + 1 \right\|_\infty \tag{A.7}$$

$$= \min_H \left\| \frac{\sqrt{2}}{\sqrt{s}} H + \frac{\sqrt[4]{-s}}{\sqrt[4]{s}} \right\|_\infty \tag{A.8}$$

Equation (A.8) is of the form

$$\gamma = \min_H \|R - X\|_\infty \tag{A.9}$$

where

$$R = \frac{\sqrt[4]{-s}}{\sqrt[4]{s}} \tag{A.10}$$

$$X = -\frac{\sqrt{2}}{\sqrt{s}} H \tag{A.11}$$

The problem now is to find $X \in \mathcal{H}_\infty$ to minimize $\|R - X\|_\infty$. From the maximum modulus theorem, only the imaginary axis need be considered, so substitute $s = j\omega$ to give

$$R = \frac{1 - j}{\sqrt{2}} \tag{A.12}$$

There are three possible options for the behavior of $X(s)$ at the origin. Either X has a pole at zero, in which case $\|R - X\|_\infty$ is infinite, X has a zero at the origin, in which case $\|R - X\|_\infty \geq 1$, or X is a constant, with either 0° or 180° phase. In the last case, the smallest value $|R(0) - X(0)|$ can have is $\frac{1}{\sqrt{2}}$, for $X(0) = \frac{1}{\sqrt{2}}$. Thus there cannot exist $X(s)$ for which $\|R - X\|_\infty < \frac{1}{\sqrt{2}}$. Since the solution $X(s) = \frac{1}{\sqrt{2}}$ results in $\|R - X\|_\infty = \frac{1}{\sqrt{2}}$, this must be an optimal solution. From Equation (A.11),

$$H = -\frac{1}{\sqrt{2}} \cdot \frac{\sqrt{s}}{\sqrt{2}} \tag{A.13}$$

and from Equation (4.16), the compensator from the output y to u is given by

$$K = \sqrt{s} \tag{A.14}$$

Appendix B

Damping Prediction from Power Flow

The $\mathcal{H}_\infty$ control design approach described in Chapter 4 yields information about the closed loop power flow achieved, via Equation (4.39). It would be useful to relate this to the closed loop modal damping achieved in the structure. For arbitrary structures, this is extremely difficult. However, for a simple structure such as the free-free beam of Example 1, in Section 5.1, a relationship between power flow and damping can be derived.

To do this, consider a *wave-packet* travelling through the structure. The wave-packet is a spatially localized disturbance, which is also narrowband in frequency, and thus can be approximated as having a single frequency. Though a disturbance that is simultaneously both spatially localized and of a single frequency is not possible, it is an approximation that can lead to reasonable results for sufficiently high frequency. The wave-packet travels at the group velocity v_g of the structure, which is a function of frequency:

$$v_g = \frac{\partial \omega}{\partial k} = \frac{2\sqrt{\omega}}{c_0} \tag{B.1}$$

where c_0 is defined in Equation (2.52). Therefore, for a beam of length ℓ, in a time

$$t_1 = \frac{2\ell}{v_g} \tag{B.2}$$

the wave-packet has travelled through the beam and back to its original position, with a decrease in amplitude associated with travelling once through the controlled junction.

The compensator absorbs a fraction $\delta(\omega)$ of the total power available. Thus in one cycle, the energy of the wavepacket decreases to

$$E(t_1) = (1 - \delta)E(0) \tag{B.3}$$

and the amplitude, which is proportional to the square root of the energy, decays to

$$A(t_1) = \sqrt{1 - \delta}A(0) \tag{B.4}$$

The modal solution is of the form

$$u(t) = \sum_i a_i \Phi_i(x) e^{(\sigma_i + j\omega_i)t} \tag{B.5}$$

The wave-packet at time t_1 in Equation (B.2) has the same shape as at $t = 0$, and only the amplitude has changed. If the disturbance is approximated to consist of only a single frequency, and if this frequency corresponds to that of mode n, then the amplitude at t_1 is related to the initial amplitude by

$$\frac{u(t_1)}{u(0)} = e^{\sigma_n t_1} \tag{B.6}$$

Comparing this with the wave solution in Equation (B.4), then one finds that the real part of the eigenvalues is given by

$$\sigma_n = \frac{\log(1 - \delta(\omega_n))}{2t_1} \tag{B.7}$$

Combining this with Equation (B.2), then

$$\sigma_n = \frac{\log(1 - \delta(\omega_n))\sqrt{\omega_n}}{2\ell c_0} \tag{B.8}$$

where the power absorbed, $\delta(\omega)$, is given by Equation (4.39) as

$$\delta(\omega) = \frac{1-\gamma^2}{|W_1|^2} \tag{B.9}$$

In particular, if the weighting function W_1 is unity, then

$$\sigma_n = \frac{\log(\gamma)\sqrt{\omega_n}}{\ell c_0} \tag{B.10}$$

Finally, the modal damping ratio ς_n is related to σ_n by

$$\varsigma_n = \frac{\sigma_n}{\omega_n} \tag{B.11}$$

Thus with equal power absorbed at all frequencies, the time constant of the beam modes increases with frequency, and the modal damping ratio decreases.